

POLITECNICO DI TORINO

Master of Science

Master's Thesis

The Effects of Coarsening Phenomenon on Foam Flow Behavior in Fractured Reservoirs



Supervisors:

Prof. William Richard Rossen *TU Delft*

Prof. Dario Viberti *Politecnico di Torino*

Ir. Kai Li *TU Delft*

Candidate:

Mohammadamin Sharifnik

Academic Year 2020-2021

*To my loved ones, who have always supported me
Specially my parents, who showed me the true love*

Summary:

Gas is very efficient for displacing oil in enhanced-oil-recovery projects because of its high microscopic-displacement efficiency. However, the process at the reservoir scale suffers from poor sweep efficiency due to lower density and lower viscosity compared to in-situ fluids. Foam substantially reduces the mobility of injected gas and hence improves the sweep. Foam rheology in 3D geological porous media has been characterized both theoretically and experimentally. In contrast, the knowledge of foam flow in fractured porous media is far less complete. Due to the gas diffusion between bubbles, foam structure will be evolved over time. There is a good understanding of coarsening behavior in a bulk foam; however, coarsening in confined geometries such as porous media is not well defined. Based on the previous studies, coarsening will cause foam lamellae to move to low energy configurations in the pore throats, leading to increased capillary resistance when the flow is restarted.

In this study, the impact of coarsening phenomena on the static foam behavior has been studied. Two different fracture geometries, including an irregular model with a mean pore diameter of 80 μm , and a regular model with a mean pore diameter of 60 μm , have been employed to conduct this study. Besides, the coarsening effects at two different foam qualities have been investigated using image analysis by ImageJ software. The results depict that the gas diffusion significantly depends on fracture geometry. The gas diffusion was ended after 5 hrs in the regular model, and the foam reached the equilibrium condition. In contrast, although after 18 hours, the coarsening rate became very slow in the irregular model, it cannot be confirmed that the coarsening rate has been stopped.

Moreover, the results show that the variation in the foam quality can alter coarsening behavior. The amount of water present can effect on coarsening rate. When there is more water, capillary pressure is expected to be lower, Plateau borders are swollen, and there is less lamella area for diffusion. Hence, the coarsening rate in the dry foam was much quicker than the wet foam. In the final step, in order to estimate the capillary pressure, the fracture models have been profiled, and these estimations have been compared for both regular and irregular models. The results indicate that the capillary pressure ranges in the regular model were almost two times larger than the irregular model.

Keywords: Foam Flow- Coarsening- Porous Media- Foam Injection- Capillary Pressure

Acknowledgement

First of all, I would like to thank Professor Bill William Rossen for all the wisdom he shared and set a great example. Besides, I appreciate all the effort that he put into teaching me the points I needed to learn during our regular weekly meetings in the past year.

Moreover, a big thanks to Ir. Kai Li for his precise and kind explanations. He has activated a hunger for knowledge and wisdom, inspiring me to plan my future and become a better individual. Thanks for everything.

Lastly, I would also like to thank Professor Dario Viberti for providing me all the knowledge and moral support I need to face my future.

Index

1	Introduction.....	1
1.1	Advantages of Foam Operations	2
1.2	Foam Texture.....	3
1.3	Foam Stability	3
	Plateau Border:.....	4
1.4	4
1.5	Fundamentals of foam flow in porous media:	5
1.6	Foam Generation in Fractures.....	8
1.7	Gas Diffusion.....	9
1.8	Foam Breakage Mechanism	9
1.9	Capillary Pressure	10
1.10	Scope of the thesis:	11
1.11	THESIS OUTLINE.....	12
1.11.1	CHAPTER 1: Introduction and literature review.....	12
1.11.2	CHAPTER 2: The effect of fracture geometry and gas fractional flow on the coarsening phenomena.....	12
1.11.3	CHAPTER 3: Capillary pressure measurements thought the fully characterized physical-model fracture.....	12
1.11.4	CHAPTER 4: Summary and recommendation.....	12
2	Introduction.....	14
2.1	The Experimental Design:.....	14
2.2	Diffusion Experiment:.....	16
2.3	The impact of the fracture geometry on coarsening:	21
2.4	Coarsening time scaling:.....	25
2.5	The impact of the foam quality on coarsening:.....	28
3	Determination of Aperture Distribution.....	33
3.1	Capillary Pressure Estimation	36
4	Summary and conclusions:.....	40

Figures

Figure 1. 1 (a) Illustration of 2nd and 3rd Plateau's laws. (b) Schema of a Plateau border and notation of r , the radius of curvature of the Plateau border [19]	5
Figure 1. 2 Cross-sectional view of cornered pores and the wetting fluid is held in the pore corners [22]	6
Figure 1. 3 Pore level schematic of foam in porous media (Tanzil, 2001)	7
Figure 1. 4 Simple schematic of foam flow into a rough-walled transparent replica. At high gas fractional flow, Lamella was observed to bridge fracture aperture, resulting in elevated flow pressure [29].	8
Figure 1. 5 Gas diffusion mechanism for bubble coalescence[32].....	9
Figure 2. 1 The Experimental setup.....	15
Figure 2. 2 The top view scheme of the fracture model.....	16
Figure 2. 3 The top view of the regular model [57]	17
Figure 2. 4 The top view of the Irregular model [57]	18
Figure 2. 5 The sample of the raw image (left side) and the processed image (right side) using ImageJ software. The image size is $0.98 \times 1.2 \text{ cm}$. Black is gas and white is water (Irregular model). ..	19
Figure 2. 6 The observation of the tiny bubbles which have not shrunk through the foam coarsening (unprocessed image after 14 hrs of coarsening). The image size is $0.98 \text{ cm} \times 1.2 \text{ cm}$ (Irregular model with the fg 0.9).	21
Figure 2. 7 a) The unprocessed image at the start of the coarsening experiment b)The unprocessed image after 24 hours of coarsening. The image size is $0.98 \text{ cm} \times 1.2 \text{ cm}$ (Irregular model).	21
Figure 2. 8 The Average Number of bubbles in both regular and Irregular models in two various locations with the fg: 0.9.....	23
Figure 2. 9 The Average Size of bubbles in both regular and Irregular models in two various locations with the fg: 0.9	24
Figure 2. 10 The top view of the coarsening behavior through the Irregular model at upstream with the fg: 0.9. The image size is $0.98 \times 1.2 \text{ cm}$. Black is gas and white is water (irregular model)	24
Figure 2. 11 The top view of the coarsening behavior through the regular model at upstream with the fg: 0.9. The image size is $0.98 \times 1.2 \text{ cm}$. Black is gas and white is water (regular model).....	25
Figure 2. 12 The ratio of the initial number of bubbles, N_0 , to the number at time t_c , $N(t_c)$ plotted as a function of time, for a single coarsening test (representative of the general behavior seen in repeat tests). The experimental data deviate from the linear trend after approximately 500 seconds [51] ..	26
Figure 2. 13 Number of internal bubbles as a function of time. A characteristic time can be defined for both bubble populations [60]	27
Figure 2. 14 The ratio of the initial number of bubbles to the number of bubbles at time t_c	28
Figure 2. 15 The Average Number of bubbles per pore in two different locations of the irregular model with the two various ranges of foam quality	29
Figure 2. 16 The Average size of bubbles in two different locations of the irregular model with the two various ranges of foam quality.....	29
Figure 2. 17 The top view of the coarsening behavior through the Irregular model at downstream with the fg: 0.4 (wet foam)	30
Figure 2. 18 The top view of the coarsening behavior through the Irregular model at downstream with the fg: 0.9 (dry foam)	31

Figure 3. 5 The Histogram graph of the regular model	33
Figure 3. 6 The Histogram graph of the regular model	34
Figure 3. 8 The capillary pressure measurements based on the gas area fraction at two various foam quality (Regular Model)	37
Figure 3. 9 The capillary pressure measurements based on the gas area fraction at two various foam quality (Irregular Model)	38
Figure 3. 10 Comparing the capillary pressure measurements in both regular and irregular models	Error! Bookmark not defined.

Tables

Table 2. 1 The conducted diffusion experiments in this study	20
Table 3. 1 The Specific aperture values for the regular model- fg 0.9 at the downstream	34
Table 3. 2 The Specific aperture values for the regular model- fg 0.4 at the downstream	35
Table 3. 3 The Specific aperture values for the irregular model- fg 0.9 at the downstream	35
Table 3. 4 The Specific aperture values for the Irregular model- fg 0.4 at the downstream	36

If you can dream it, you can do it

[WALT DISNEY]

Chapter 1

Fundamental of Foam

1 Introduction

Foam consists of gas bubbles dispersed in a continuous liquid phase and treated with variable density and viscosity as homogenous fluid [1]. Since foams contain more than a minimum amount of gas solution interface, they are considered unstable systems. This interface represents surface free energy, the product of the surface tension, and the foam's interface area. Once a foam membrane breaks down and the liquid coalesces, surface-free energy declines. Hence the decomposition process of foam will be spontaneous. Since the liquid phase is frequently denser than the gaseous phase, the prior appears to detach or drain from the main foam body unless it circulates or agitates. This drainage contributes to the instability of the physical characteristics of height and time preceding the rupture. The surfactant plays a crucial role in film stabilization, entrapping the gas bubbles, allowing the foam structure to persist. The fluid, the denser phase, always tends to drain out of the main body unless there is frequent agitation due to differences in density between the two foam phases. Foams might have relatively high viscosity values, a value greater than the two constituents, at a constant shear rate.

Furthermore, the foam has a density lower than that of the liquid phase. Its high viscosity ensures efficient transport of cuttings in foam drilling, and low density allows under-balanced conditions. Foam drilling has resulted in enhanced productivity, increasing drilling rate, and reducing operational complexity such as lost circulation and differential stuck piping, and it gives improved formation evaluation in drilling [2]. While foam drilling is a valuable method due to its very low density, besides the high carrying capacity of cuttings, characterization of foam properties under drilling conditions is still incomplete, and this is most likely to be a barrier for operators to make use of this technique [3]. The application of foam fracturing fluid may control fluid loss into the formation, and it can provide excellent fluid recovery immediately after treatment. In well-stimulation, clean-up, and fishing, foam was also successfully used in the oil and gas fields. The use of foam as a drilling fluid has been shown to have a powerful lubrication effect, with a lubricity index between water base mud and oil-based mud [3, 4].

Foams are generally characterized by their quality, as defined in equation 1.1 [4];

$$fg = \frac{V_g}{V_g + V_l} \times 100 \quad 1 - 1$$

where V_g is the gas volume, V_l is the liquid volume, and fg is the foam quality in percentage. A high-quality foam (dry foam) contains more gas than a low-quality foam (wet foam). The size and distribution of the bubbles are quantified as "texture." In the foam drilling operation, a fine-textured

foam has smaller and spherical bubbles, and large and polyhedric bubbles reflect coarse foam. In these terms, fine foam is a low-quality sphere foam, and coarse foam is a high-quality polyhedric foam [4]. The continuous liquid phase transforms into a discontinuous situation if the foam's quality reaches a threshold level and results in mist formation. It should be remembered that the maximum limit for the stable foam is not determined, and it depends on the shear rate. Okpobiri and Ikoku, in 1986, discovered that foam had collapsed at a quality of 94 to mist, at a shearing rate below 5000, but at a shearing rate above 5000, it would have stayed at a quality of up to 96 [5]. Beyer et al., 1972, claimed that foam had become unstable at fractions of liquid volume from 0.02 to 0.03 and that foam tended to flow as intermittent foam and gas slugs when the quality exceeded 98. For foam stability, the liquid phase's composition with the gas phase is essential [6]. In the study by Rusell in 1993, he discovered that foam with good bubble stability was only developed without polymers by surfactant solution at 99.1, known as "stable foam." On the other hand, with polymers' addition, it was observed that stable foams were developed in 99.65 quality. Until the quality reaches 55%, the dispersed gas bubbles' interaction within the foam structure will remain intact [7].

1.1 Advantages of Foam Operations

High viscosity and low-density foams may give the following positive results (Baroid Fluids Handbook 1998);

- ❖ Compared to air (an annular velocity of 3000ft/min is typically needed for air drilling) or mist drilling, foam is much more effective at much lower annular velocities in removing cuttings. Foam injection rate in the internal phases is lower than those needed for air or mist drilling.
- ❖ Due to the low density in the foam design, underbalanced conditions inside the wellbore can undoubtedly be achieved. The penetration rate for foam drilling is significantly higher than for conventional mud drilling.
- ❖ With higher annular pressures, potential mechanical wellbore instability could be reduced during foam drilling, while possible borehole erosion could be overcome at low annular velocities.

Air is the most commonly used internal phase for foam drilling in under-balanced operations due to its availability. Gas flow is mixed with a surfactant solution, and the mixture is pumped into the drill string. After being produced in a foam generator, the foam will be produced while still flowing through the bit.

Foams, as mentioned above, are complex mixtures of gas, liquid, and surfactant, the rheological properties of which are strongly influenced by parameters such as absolute pressure, foam quality,

temperature, texture, foam/channel-wall interactions, liquid phase properties, and the type and concentration of surfactant [8]. The rheology of foams is also more complicated than that of other basic drilling fluids. However, the capacity to lift large volumes of produced liquids is most likely the primary reason for its use, contrary to the difficulty of the rheological specification of foams as underbalanced drilling fluid.

1.2 Foam Texture

The shapes of the bubbles are used to classify the foam. As a result of the minimum-energy principle, in bulk foam, bubbles tend to be spherical in shape. This type of foam is referred to as sphere foams if the bubble concentration is high and small or if the foam is newly generated. Besides, polyhedral bubble foams are considered to be polyhedral foams. The amount of liquid volume in sphere foams is higher than polyhedral foams, as is understood from geometrical relations. This is due to the fact that, in the case of polyhedral foams, there must be more order than that of spherical foams. For spherical foams, the liquid phase is thicker than for polyhedral foams. Ideal foam for oil extraction/reservoir simulation purposes is needed to be as preferably polyhedral as possible; the bubbles may have as many as 12 sides [9].

1.3 Foam Stability

In order to ensure high sweep efficiency, the foam produced in the field must be sufficiently stable to propagate through the formation. Friedmann and Jensen (1986) discovered that a high-velocity gas injection strategy could enhance foam stability. Increased shearing between gas/surfactant/porous media results in smaller, uniform bubbles, distinguished by high-quality foam [10]. When CO₂ is used to control mobility, this logic does not apply. CO₂ foams with high quality could be extremely immobile, leading to a sharp drop in the reservoir pressure. Instead, a low-quality foam may be suitable as it can be pumped for an extended period as CO₂ progressively reaches oil mobility [11]. Following are some main factors affecting the stability of the foam. Limiting capillary pressure is found to destabilize foam film produced inside a porous medium. Capillary pressure increases with declining wetting fluid saturation during foam flooding, similar to a water-wet reservoir drainage system. The reduction of the water supply from the Plateau borders to the lamellae results in the film's thinning [12]. Approaching a limiting capillary pressure, P_c^* , the work needed to destabilize a film is minimal, and minor mechanical disruptions or thermal variations are sufficient to trigger a rupture [13]. A coarse, unstable foam texture results from P_c^* , which depends on the form of surfactant, its concentration and electrolyte content [14]. Diffusion can lead to foam coalescence and is characterized as a process by which one location's physical properties are transferred to another [15]. The pressure difference between large and

small bubbles in a foam causes the gas to diffuse smaller bubbles into larger bubbles through the lamella [16]. Gas compressibility effects are stated to impact foam flow in porous media. If there is a minimum pressure gradient, foam moves as bubble trains at low-pressure gradients and $(\nabla P)^{min}$ can be obtained by the following formula [17]:

$$(\nabla P)^{min} = (\Delta P)^{avg} n_L \quad 1 - 2$$

where $(\Delta P)^{avg}$ is the average differential pressure between each lamella in the train and n_L is the number of lamellae per unit length. The positive pressure difference between each bubble of the train needs Lamella to flow. However, an increased $(\nabla P)^{min}$ value due to gas-filled bubble compression can cause unequal $(\Delta P)^{avg}$ distribution within the bubble train, resulting in random pressure fluctuations and frequent bubble separation. By occupying pore throats, compressible foams increase the flow resistance and depend on the bubble's size, the presence of trapped gas, and the length of the bubble train [17].

1.4 Plateau Border:

Definition of foam in a porous medium as written by Rossen: "*a dispersion of gas in liquid such that the liquid phase is interconnected and at least some of the gas flow paths are blocked by lamellae*" [18]. The boundary between the lamellae or a solid is a liquid prismatic region called a plateau border, as shown in figure 1.1. There are three laws known as Plateau's laws from the name of the Belgian physicist who stated them in 1873 [19, 20]:

1. Two bubbles are separated by a liquid film of constant average curvature.
2. Three films join in channels called the Plateau border and form 120° angles.
3. At each node, four Plateau borders intersect and form 109.5° angles.

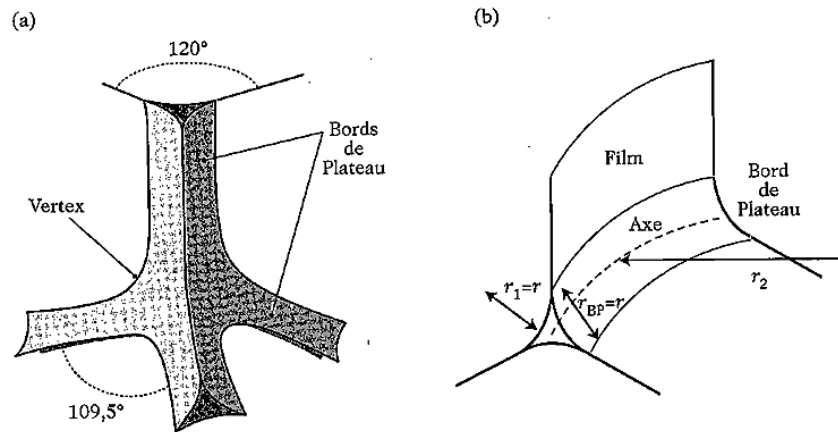


Figure 1. 1 (a) Illustration of 2nd and 3rd Plateau's laws. (b) Schema of a Plateau border and notation of r , the radius of curvature of the Plateau border [19]

1.5 Fundamentals of foam flow in porous media:

Foam can be injected into geological formations for a wide range of applications: enhanced oil or gas recovery (EGR), aquifer and soil remediation, CO₂ surface sequestration and acid well diversion. The goal of most applications is to maximize the volume of the injected fluid reservoir or to block one layer in order to inject into another. The geological heterogeneity of the formation, the density differential between gas and resident fluids, and the low viscosity of gas compared to resident fluids all contribute to the injected gas's sweep efficiency [21].

In porous media, the pores' connectivity and geometry can play an essential role in the foam flow behavior. Various characteristics can be defined for a porous medium, which might be crucial for foam flow. The aspect ratio of the body to throat size is one of the critical parameters, which significantly impacts the destruction or generation of foams. Secondly, pores are not cylindrical but have corners. The wetting fluid for large pores resides in the corners of pores occupied by gas and in thin wetting films covering the pore walls (Figure 1.2). In the central part of the large pores, the non-wetting phase can be present, and tiny pores are where the wetting phase can continuously occur. Third, the capillary pressure is determined by local wetting-phase saturation and interfacial tension when the flow rate is extremely low, and the capillary forces dominate. Local variations in capillary pressure appear to equalize through the interlinked, continuous wetting process. The large interconnected pore channels are the place through which the non-wetting phase starts to flow. This is due to the pressure gradients in the wetting phase in the interconnected narrow channels and pores occupied in the wetting liquid's corners.

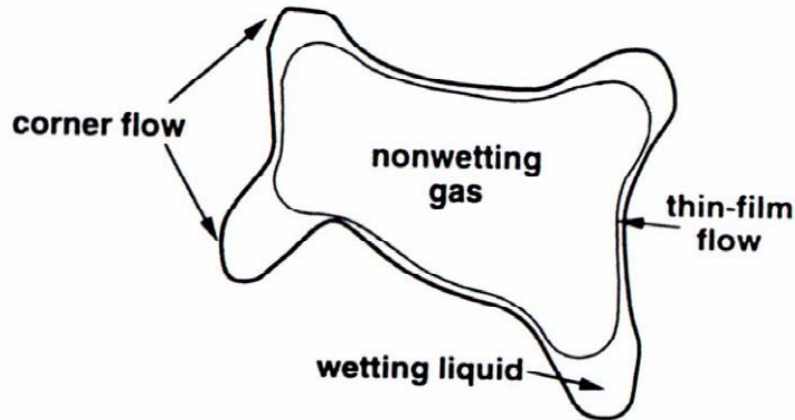


Figure 1. 2 Cross-sectional view of cornered pores and the wetting fluid is held in the pore corners [22]

On the other hand, the bubbles and lamellae span pores are entire pores when the characteristic pore size is equal to or less than the diffused gas bubbles' characteristic size. The pore-spanning bubbles are widely distributed at low gas fractional flow, separated by thick wetting fluid lenses or bridges. At high gas fractional flow, the pore-spanning bubbles are in direct contact, separated by lamellae. [23], define this morphology of direct contact as the individual-lamellae regime. While both bulk foam and individual-lamella foam can exist in theory, sizes of effluent bubbles equal to or greater than pore sizes are typically reported. It is now widely agreed that single bubbles and lamellae span the pore space of most porous media undergoing foam flow in the absence of fractures. Figure 1.3 depicts the schematic of foam flow in porous media. As a continuous or discontinuous phase, gas may flow or even trap. In discontinuous-gas foam, the entire gas phase is made discontinuous by lamellae, and no gas channels are continuous over sample-spanning dimensions. Gas is encapsulated in small packets or bubbles by surfactant-stabilized aqueous films. The medium contains interconnected gas channels in continuous gas foam, which are continuous over macroscopic distances by lamellae. In general, discontinuous foam forms during coinjection of gas and surfactant solution provided that the wetting-phase saturation and flow rate are adequate for foam generation. If the wetting phase's saturation is sufficiently low, the lamella generation rate could be less than that of rupture, and continuous gas flow paths may occur.

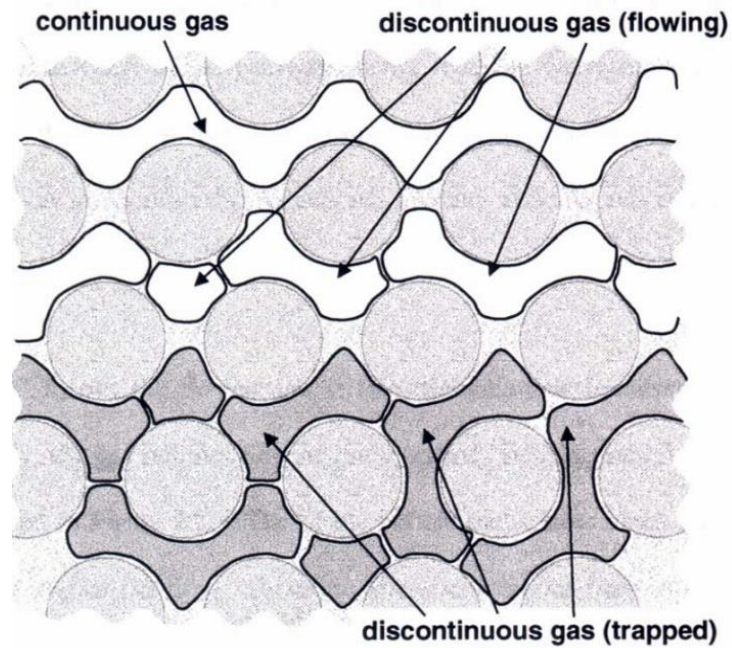


Figure 1.3 Pore level schematic of foam in porous media (Tanzil, 2001)

Figure 1.3 illustrates the pore-level microstructure of foam flow over porous media. The wetting surfactant solution flows as a separate phase in the narrow pore spaces due to capillary forces' dominance. Minimal wetting liquid transports with the gas as lamellae. Therefore, if the foam is present, the relative permeability of the wetting phase, as a function of saturation, remains unchanged. When both flowing and trapped gas are present, foam is transported in large pores due to the greater resistance of bubbles in the smaller pores. The relative permeability of foam is a function of the gas trapping; the trapped gas saturation reduces it. The foams, moving through the largest pores, parade as trains of bubbles, and, in some cases, they are destroyed and recreated.

Foam can be divided into "weak" and "strong" foams. In the case of "weak foam" without moving lamellae, it is vital to increase the saturation of trapped gas to minimize gas's relative permeability, contributing to the disruption of the gas pathways. The trapped gas reduces mobility; however, the rest of the gas flows continuously. "Strong" foam flows through a different process. The lamellae cause the flowing gas to be discontinuous. Then the bubble trains face a much higher resistance than in the continuous flow of gas. The apparent viscosity of discontinuous foam is typically much higher than that of continuous foam. Reducing the relative permeability of the gas and increasing the gas's apparent viscosity can significantly decrease the foam's mobility. In general, the most critical parameters affecting foam trapping and mobilization are pressure gradient, gas velocity, pore geometry, and bubble size. Increasing the pressure gradient can open new channels occupied by moving or trapping gas [24, 25].

1.6 Foam Generation in Fractures

Foam studies have been conducted in several fractured structures, ranging from idealized fracture models characterized by smooth rock surfaces and homogeneous aperture distribution to heterogeneous rough-wall systems. Lamellae can be created through three main mechanisms [26, 27]. Some researchers assume Snap-off to be the dominant foam-generation mechanism [28]. It occurs at constrictions in the flow path with a sudden change in capillary pressure. A fall in capillary pressure will result in water flow to the constriction's neck, followed by the snap-off and separation of the gas bubbles [29] studied foam flow into a rough-walled transparent replica. According to this study, the foam was generated in two ways; in-situ by the coinjection strategy of nitrogen and surfactant injection into the fracture and using the Berea sandstone pre-generator. Snap-off was the primary foam-generation mechanism during their experiments, and tracking the size and shape of bubbles showed that in-situ foam experiments had approximately four times larger bubbles compared to pre-generated foam. At high gas fractional flow, large bubbles were observed to become more stationary. As shown in Figure 1.4, lamellae bridged the fracture aperture and resulted in elevated flow pressure due to increased flow resistance within the fracture.

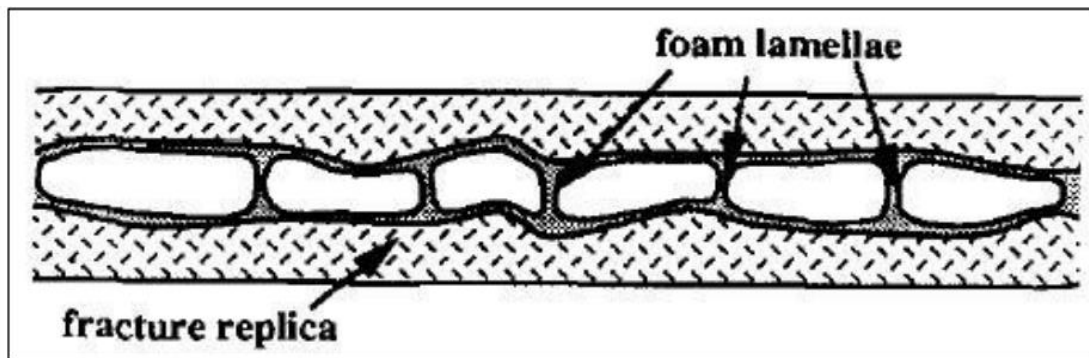


Figure 1. 4 Simple schematic of foam flow into a rough-walled transparent replica. At high gas fractional flow, Lamella was observed to bridge fracture aperture, resulting in elevated flow pressure [29].

The comparable results of gas and surfactant solution coinjection into a fractured marble network with diverse fracture aperture variations were investigated [30]. Lamella generation by snap-off was observed in large vugs, and the final foam resistance was calculated at $f_g = 0.90$. Experiments coinjecting gas and surfactant solution into a 2D silicon micromodel representing a fractured network [31] have confirmed that snap-off is the dominant foam generation on a micro-level. Snap-off was observed with a high-resolution camera at sites where the wetting phase (water) accumulated in pores initially filled with gas. There were also snap-off sites in places where the low-permeability matrix opened up to high permeable fractures. The lamella was found to follow

only a path, usually with the highest pore throat radius, preventing foam generation from lamella division to occur.

1.7 Gas Diffusion

For trapped foam bubbles, the gas on the concave side of an interface has a higher pressure than that on the convex side. The pressure difference drives the gas to diffuse from the concave side to the convex side through the liquid film. The gas diffusion mechanism is thought to be less critical than the capillary suction mechanism in foam coalescence in porous media (figure 1.5) [32]. The effects of the gas diffusion rate on the stability of the foam came from two aspects. First, gas diffuses across lamellae from greater pressure to lower pressure. Second, the gas inside the bubble is partially dissolved in the liquid film. Gas diffuses through a lamella by dissolving on one side, diffusing through liquid to the other, and evaporating on the other side. According to figure 1.5, the curvature of the interface between the two bubbles reflects the pressure difference between them.



Figure 1. 5 Gas diffusion mechanism for bubble coalescence[32]

1.8 Foam Breakage Mechanism

Foam stability is referred to its capability of time to maintain its structure for a considerable period, while it is not thermodynamically stable. Four main mechanisms are affecting the texture of foam over time: (1) gas diffusion (2), liquid drainage (3), interaction with oil, and (4) capillary suction [18, 33, 34]. The curvature of the neighboring interfaces may not be zero, and so gas is compressed differently within the bubbles. The gas is at a higher pressure in smaller foam bubbles than in coarser ones. In bulk foam, the bubble's radius regulates the bubbles' pressure due to the Young-Laplace equation; more generally, it is the curvature of the interface between bubbles. The pressure difference ΔP across the lamellae relates to the surface tension coefficient σ and the main curvature radii r_1 and r_2 according to the following equation [35]:

$$\Delta P = 2 \sigma \left(\frac{1}{r_1} + \frac{1}{r_2} \right) \quad 1 - 3$$

As a result, gas diffuses from small, higher-pressure bubbles to larger, lower-pressure bubbles, ultimately leading to the vanishing of small, neighboring bubbles [36-38].

The second mechanism is fluid drainage, which is a multi-step process that comprises multiple steps. (a) fluid flows by capillary suction from the lamellae to the plateau border, i.e., the intersection of the lamellae; b) Water is released from foam bubble coalescence; (c) eventually fluid drains through the Plateau borders under gravity, resulting in fluid accumulation in the lower foam layer [39]. Gravity and capillary suction are the critical mechanisms in controlling the whole system, which can finally affect film rupturing when the lamella thickness becomes lower than a particular value [40].

The adverse effect of oil on foam stability results from direct surface interactions between oil and foam, leading to aqueous film thinning and rupture. It is another significant obstacle to the successful use of foam application in oil displacement [41-43]. The negative influence of oil on the stability of foam depends on surfactant and oil properties. It is worth mentioning that light oil has a more negative effect on foam stability than heavy oil [44-46]. Besides, as the capillary pressure (the pressure around the gas and surfactant solution interface) increases in the capillary suction: the thickness of the lamellae decreases, and it breaks after passing a threshold.

1.9 Capillary Pressure

When two immiscible fluids are present in a thin capillary tube or a pore, the adhesive forces lead the wetting fluid to curve along the wall. The meniscus between these two fluids can create an angle with the pore wall called the contact angle. The molecular pressure difference across the interface of the two fluids can be determined by capillary pressure. Capillary pressure can also be defined as the pressure difference between the wetting and non-wetting phases [47].

$$P_c = P_{nw} - P_w$$

1 – 4

where P_c is the capillary pressure, P_{nw} is the pressure of the non-wetting phase, and P_w is the pressure of the wetting phase. The difference in pressure arises from the interaction between the adhesive force and the cohesive force.

Capillary pressure can be related to the size of the Plateau borders. Due to the interfacial curvature, the pressure is lower and the film is thicker in the Plateau border, so that a sucking effect on the liquid from the center of the film to its periphery occurs (Pugh, 2005).

There are three principle forces in a porous medium in the presence of two immiscible fluids. The viscous force (VF), the force of gravity (GF), and the capillary force (CF) Skarestad and Skauge [48]. The capillary force captures the non-wetting phase in the pores and makes recovery of the non-wetting phase more difficult. The viscous force drives the oil non-wetting phase. The gravitational force can both stabilize a front and trigger segregation. A dimensionless number can be derived from these

forces, which is called the capillary number. This term expresses the ratio of viscous force and capillary force and can be described as [49]:

$$N_{vc} = \frac{VF}{CF} = \frac{u_w \cdot \mu_w}{\sigma_{n/w}} \quad 1 - 5$$

where N_{vc} is the capillary number, u_w is the superficial velocity of water, μ_w is water viscosity and $\sigma_{n/w}$ is the interfacial tension between the non-wetting phase and water.

1.10 Scope of the thesis:

Foam is not a single phase; in foam, two phases flow simultaneously. There is always a battle between the viscous and capillary forces during this flow. Therefore, this competition can result in gas trapping. One of this thesis's objectives is defining the geometrical fracture parameters responsible for trapping the non-wetting phase (gas). A pre-generated foam in two different fracture geometries was studied to investigate the coarsening phenomena' impact on the foam flow behavior. Similarly, we monitored gas diffusion's effect in two ranges of fractional gas flow and total superficial velocities.

Once the foam is generated, we injected foam into the fracture so that the entire fracture's pressure became stable. Since fractures on the scale of a reservoir are most likely to reach hundreds of meters and expand in the whole reservoir thickness, it is essential to investigate the foam propagation and the rate of generation/destruction of foam lamellae. However, the main focus of this project is to study the static foam when the injection has been stopped. The pressure gradient has been recorded throughout the whole part of the fracture to track the gas diffusion. Image analysis has been used to make a comparison between foam texture and pressure gradient.

To fulfill our research objectives, we designed an experimental fracture apparatus made of glass plates. These models have been used to study foam and two-phase flow in fractures [50]Pruess and Tsang, 1990; Fourar et al., 1992; Pieters and Graves, 1994; Chen et al., 2004; Yan et al., 2006; Qian et al., 2011). the following design criteria are the reasons why we have used such the model for our study:

- To visually monitor the generation of foam and foam texture.
- To monitor foam stability over a significant distance
- Provide water-wetting surfaces.
- To record various pressure measurements along the fracture to link the texture to the pressure gradient.

1.11 THESIS OUTLINE

1.11.1 CHAPTER 1: Introduction and literature review

In order to understand the concept of foam injection in naturally fractured reservoirs, some published information on this particular subject has been provided. This summary is a recap of crucial details on foam flow fundamentals in porous media to the effect of the coarsening phenomena on foam flow behavior.

1.11.2 CHAPTER 2: The effect of fracture geometry and gas fractional flow on the coarsening phenomena

In the first part of this chapter, to determine the diffusion rate at the various fracture geometries, the average number of bubbles per pore, gas area fraction, and the size of bubbles have been investigated. Similarly, in the second part, the coarsening rate in different fracture geometries has been studied. The approximate starting and ending of the diffusion processes for these models had been observed. In the second part, the effect of gas fractional flow and total superficial velocities on the coarsening phenomena have been studied.

1.11.3 CHAPTER 3: Capillary pressure measurements through the fully characterized physical -model fracture

This chapter focuses on capillary-pressure estimations of the two fracture models. In this chapter, using MATLAB software, the two different fracture profiles have been modeled. Capillary pressure and gas saturation estimations play a crucial role in investigating the coarsening phenomena in a naturally fractured reservoir.

1.11.4 CHAPTER 4: Summary and recommendation

The summary of all the results is presented in the chapter.

Chapter 2

The Effect of Fracture Geometry and Foam Quality on the Coarsening Phenomenon

2 Introduction

Due to the gas diffusion between bubbles, foam structure will evolve over time. There is a good understanding of coarsening behavior in a bulk foam; however, coarsening in confined geometries such as porous media is not well defined. Based on the previous studies, coarsening will cause foam lamellae to move to low-energy configurations in the pore throats, leading to increased capillary resistance when the flow is restarted. [51]

Coarsening derives from the pressure difference between two neighboring bubbles, with gas diffusing from the higher pressure bubble to the lower pressure bubble at a rate determined by Fick's law [51, 52]:

Rate of gas transfer across lamella = mass transfer coefficient \times film area \times pressure difference.

For a two-dimensional foam, any liquid film between two bubbles has a curvature radius, r , which determines the pressure difference, ΔP , between the two bubbles. The pressure difference can be defined as [53]:

$$\Delta P = \frac{2\sigma}{r} \quad (1)$$

where σ is the surface tension of the liquid.³ In a perfectly monodisperse two-dimensional foam, all the bubbles have six sides, and the internal pressure is constant for every bubble. In a polydisperse two-dimensional foam, the smaller bubbles typically have fewer sides (<6) and higher pressures, and the larger bubbles have more sides (>6) and lower pressures. Gas diffusion is then in the direction from the smaller bubbles to the larger bubbles, with the consequence that the smaller bubbles disappear entirely.

2.1 The Experimental Design:

Two physical-model fractures have been designed to investigate the impact of coarsening on foam flow behavior. There are various experimental approaches to study foam flow behavior, including using microfluidics devices in cores to represent flow in fractures [31, 54-56]. Microfluidic devices have distinct channels, usually rectangular in cross-section, which do not represent an aperture that varies continuously in 3D [57]. Another method is to design a fracture apparatus made of glass plates. Model fractures based on glass plates have been used to study flow in fractures [28, 58] [59]. The clarity of the glass enables us to monitor the foam flow and assess the saturation during the experiment. The variety of commercially available roughened glass makes it possible to test a wide range of types and scales of roughness. Therefore, we designed two different model fractures using

glass plates fabricated at Delft, The Netherlands. The size of the fractures is $100 \times 15 \text{ cm}^2$. Each consists of a roughened plate representing fracture wall roughness and a smooth top plate to allow direct observation of the flow and measurement of saturation. Figure 2.1 shows the experimental setup of our study.

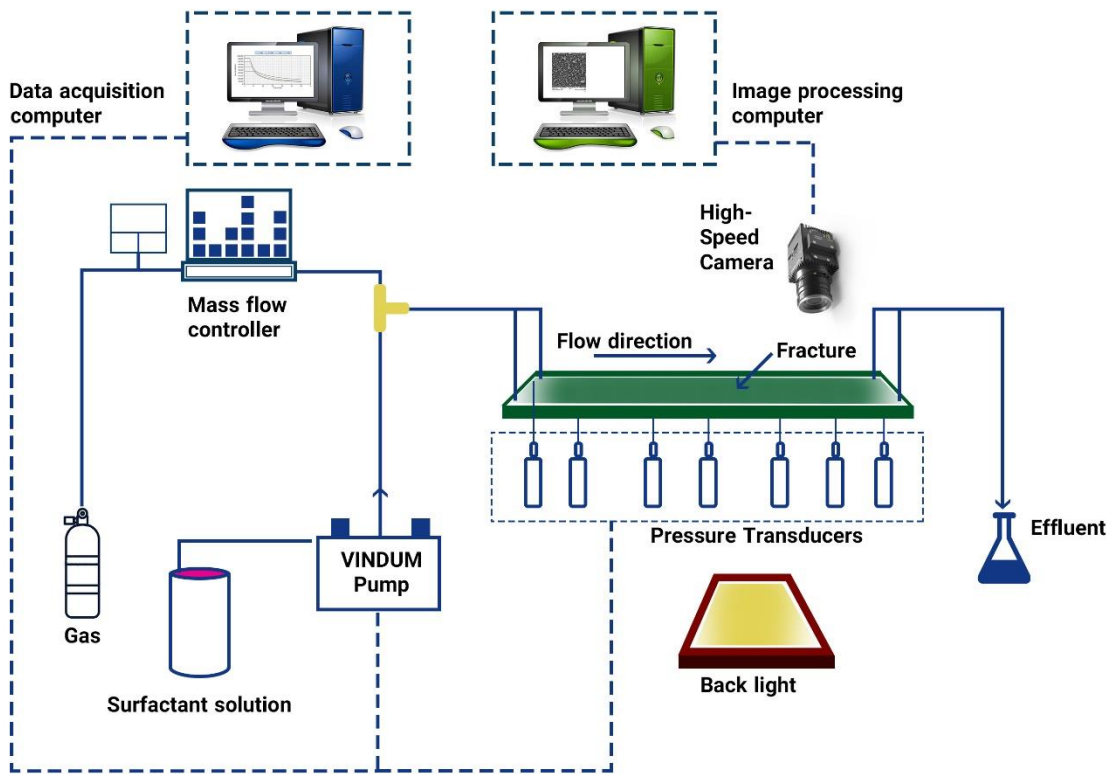


Figure 2. 1 The Experimental setup

In order to create a fracture model, the two glass plates are aligned opposite each other and are bonded around four edges using Silicon rubber. The model is then mounted in an aluminum clamping frame. The area between the two plates indicates the opening of the fracture. Eleven holes have been positioned for foam injection and fabrication along with the fracture model. These holes are connected to the pressure transducers, allowing to measure pressure across the entire channel system. The sensors are silicon on-chip, signal conditioned, and temperature compensated. The sensors are connected to a data acquisition unit and a computer, where pressure is recorded every second. The glass plate model is divided into six 18-cm-long sections, except for sections 1 and 6, respectively 7 cm long and 15 cm long. Besides, there are two toughs, one in the inlet and another one in the outlet, with the dimension of $12 \times 2 \times 0.04 \text{ cm}^3$. The first one in the inlet allows the foam to flow, and the second one at the outlet prevents flow from converging on a single point (Figure 2.2).

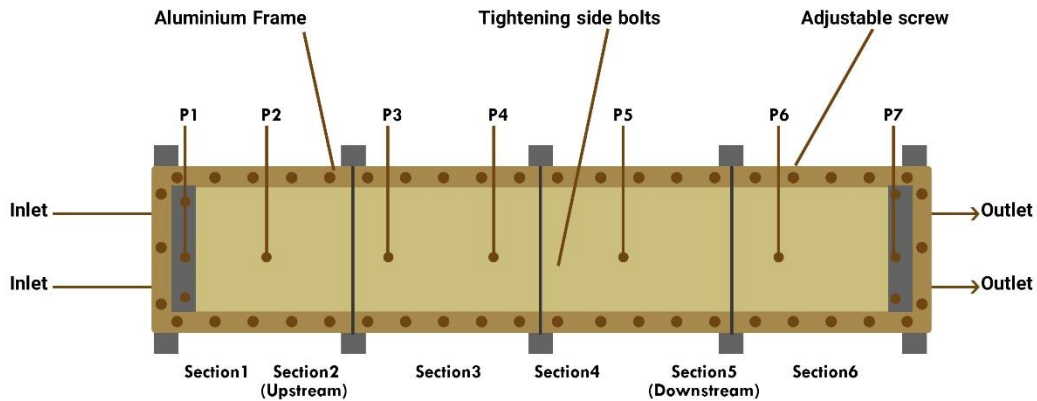


Figure 2. 2 The top view scheme of the fracture model

To monitor the foam flow behavior inside the fracture plate, a light source besides a high-speed camera (Photron Fastcam UX 50) has been used, capturing images up to 160,000 fps. A backlight device (Val LED lightning, VL-CB-CL) is employed as a source light. Moreover, image acquisition can be operated through a computer. The entire setup is located inside a tent to exclude potential external and internal reflections. The surfactant used was a Sodium C14-16 Alpha Olefin Sulfonate (AOS) (Bioterge AS-40K), a surfactant commonly used in foam core floods for Enhanced Oil Recovery (EOR) research, and the solution contained 1 wt % total active surfactant in demineralized water. The surfactant solution was injected through a pump (VINDUM Engineering, model VP1-12K). A mass flow controller (Bronkhorst Nederland BV, F230M) has been used for gas injection.

2.2 Diffusion Experiment:

In this study, to investigate the effect of gas diffusion on foam coarsening, two fracture models with various apertures have been designed. The first model was etched with an irregular pattern that formed a porous medium, with a mean pore diameter of 80 μm , and the second model with a mean pore diameter of 60 μm with a regular pattern. Each model fracture was represented by its aperture distribution as a two-dimensional network of pore bodies (maximum in aperture) connected to the throats (saddle points between pore bodies).

In this study, to scan the fracture models, a chromatic profiler (Precitec Optronic GmbH, Philips Innovation Services, Eindhoven, The Netherlands), having a height resolution of 0.5 μm and a scanning window of 50 \times 50 μm , has been used [57]. The device used a chromatic aberration lens system, and the reflected color is a height indicator. Light scattering makes it difficult to assess the height at specific points for the optical profilers. It reliably captures height at positions with small slopes that are relatively shallow but not at very steep slope positions. Fortunately, the areas captured

include height maximums, minimums, and saddle points, i.e., the most appropriate positions for our purposes [57]. The instrument restores the missing data using a smoothing algorithm. Figures 2.3 shows the results of the areas measured in the regular model, and figure 2.4 represents the Irregular model. The height of the surface varies considerably between the samples. The zero value is an arbitrary height defined as the original height values minus the minimum height value. Pore bodies defined at local minima of height in the roughened plate and pore throats at saddle points between pore bodies.

According to figure 2.3, a patch size of $1\text{cm}\times 1\text{cm}$ was considered for the regular model. In the regular model, each pore body has one local minimum and was connected to other four pore bodies through pore throats. While, the irregular model has multiple local minima for each pore body and the patch size of $4\text{cm}\times 4\text{cm}$ was taken into account (figure 2.4). Besides, the maximum z value in the regular model is around $120\ \mu\text{m}$, and in the irregular model is $209\ \mu\text{m}$.

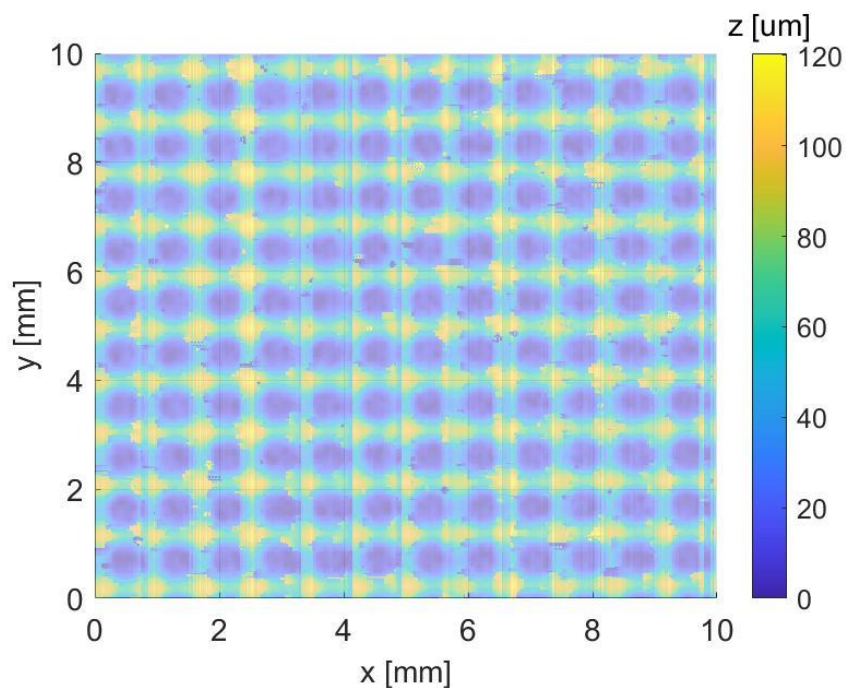


Figure 2. 3 The top view of the regular model [57]

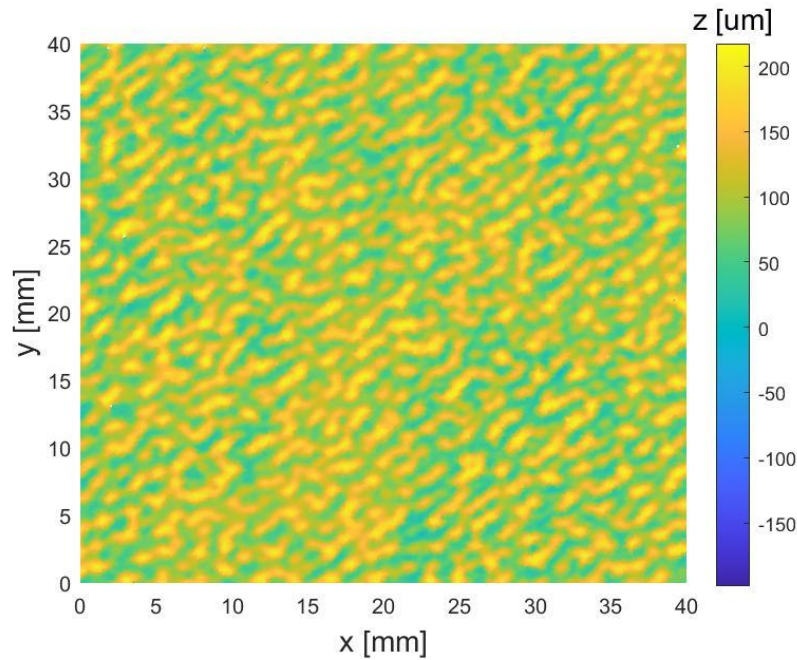


Figure 2. 4 The top view of the Irregular model [57]

In the first step, the effect of geometry on coarsening phenomena will be discussed. In order to predict the impact of diffusion along the fracture length, two positions, one representing the upstream and the other one downstream, have been selected. All the results are based on image analysis, which has been done through these two sections (Figure 2.2).

A mixture of demineralized water and surfactant solution with 1 wt % and nitrogen (N₂) was used to prepare the required foam to be injected through the pre-generation injection strategy. Therefore, water and surfactant solution have been mixed, and the inlet and outlet valves should be opened to allow the injection to begin. For the regular model, foam is injected with a superficial velocity of 1.2 mm/s. However, for the irregular model, we increased the velocity up to 2 mm/s. The pressure distribution over the entire fracture model has been monitored. Once the pressure along the upstream and downstream become almost stable, a steady-state condition will be reached. The injection is continued for an hour to establish steady the foam flow in the entire fracture model. In the next step, to investigate the coarsening phenomena on the static foam, it is necessary to stop the injection and then close the inlet and outlet valves to keep the foam inside the fracture model for further investigation. The final step is to place the camera to capture raw images from foam flow behavior over time. Based on the geometry, the coarsening can have different effects on gas bubbles.

In this study, a digital image-processing software, ImageJTM, is used for analyzing the foam images obtained during flow tests. The 8-bit colored foam images were captured during tests. After that, the images are converted to binary images using a procedure called thresholding. Figure 2.5 (left side)

depicts a raw image before and after processing. According to figure 2.5 (right side), the black color represents the gas phase, and the white represents the water phase.

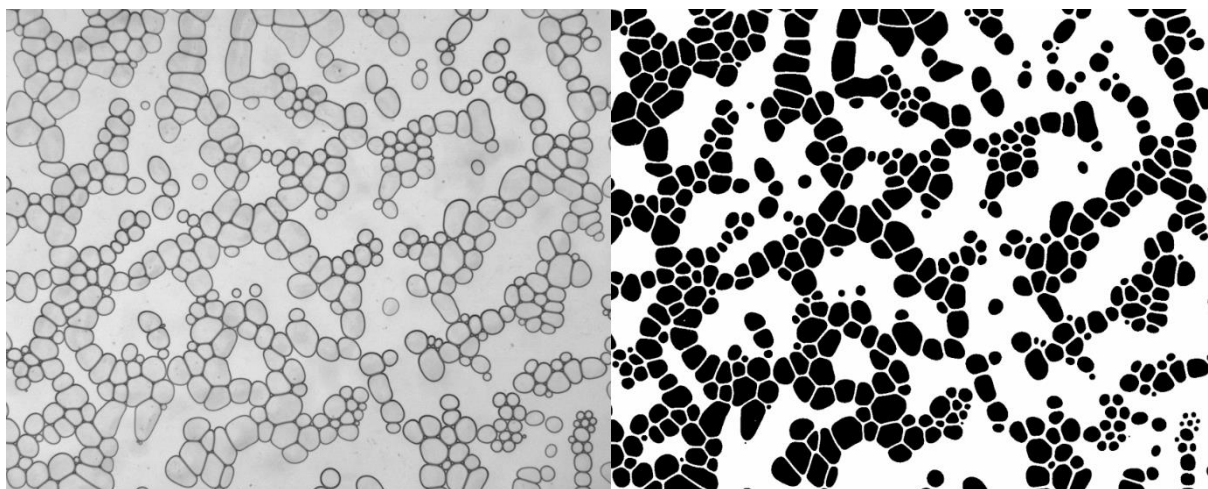


Figure 2.5 The sample of the raw image (left side) and the processed image (right side) using ImageJ software. The image size is 0.98×1.2 cm. Black is gas and white is water (Irregular model).

The starting point of coarsening, ending time, and coarsening rate are essential parameters that should be taken into account. Hence, the time of the coarsening experiment is quite challenging.

According to table 2.1, several tests have been run to determine the appropriate time of the coarsening tests. First, the test was started with 7 hours of coarsening, which means, after stopping the injection, the camera captured the static foam for 7 hours, continuously. Since the camera's maximum storage capacity is to capture up to 8600 images, the time interval of capturing should be set before starting the coarsening experiment. As clearly shown in figure 2.6, some tiny bubbles have not yet shrunk, indicating that the gas diffusion is not ended yet. Therefore, to further analyze the coarsening phenomenon, it was necessary to increase the duration of the experiment. In the next test, we increased the time duration to 14 hours. Since some tiny bubbles were still observed, so we increased the duration time to 36 hours and then in the final step to 72 hours. After more than two hundred images were processed, the rest of the tests continued with a time duration of 24 hours as the experiments' optimum time duration. Finally, four tests in two various locations have been selected to study the coarsening effect on the static foam. In the following part, the impact of fracture geometry on the coarsening behavior will be discussed.

Table 2. 1 The conducted diffusion experiments in this study

Experiment	Fracture Model	fg	Section Number	Superficial velocity (mm/s)	Diffusion Time (Hrs)	Image time interval (S)	Image Resolution (mm/pixel)	Patch Size (cm ²)
Test 1	Regular Model	0.9	2 (Upstream)	1.2	24	15	0.0096	0.98 × 1.2
			5 (Downstream)			15		
Test 2		0.4	2 (Upstream)			15		
			5 (Downstream)			15		
Test 3	Irregular Model	0.9	2 (Upstream)	2		10		
			5 (Downstream)			10		
Test 4		0.4	2 (Upstream)			15		
			5 (Downstream)			15		

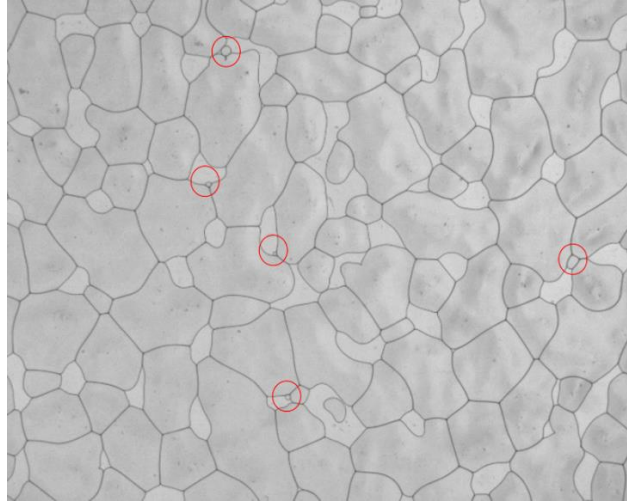


Figure 2. 6 The observation of the tiny bubbles which have not shrunk through the foam coarsening (unprocessed image after 14 hrs of coarsening). The image size is 0.98 cm × 1.2 cm (Irregular model with the fg 0.9).

2.3 The impact of the fracture geometry on coarsening:

During coarsening, gas diffuses through lamellae from bubbles at higher pressure to bubbles at lower pressure, the bubble shrinks and loses neighbors and consequently empties more and more quickly. In this way, bubbles disappear, one after another, so the average size of those which remain increases [19]. Finally, there is only one large bubble remaining, which contains all the gas. Figure 2.7 depicts the foam flow behavior after 24 hours of coarsening. This coarsening mechanism and the resulting foam structure are generic. However, the rate at which coarsening occurs depends on the particular characteristics of the system being considered; for foam, it depends on the liquid fraction, the average bubble size, and the physical chemistry of the gas and the liquid.

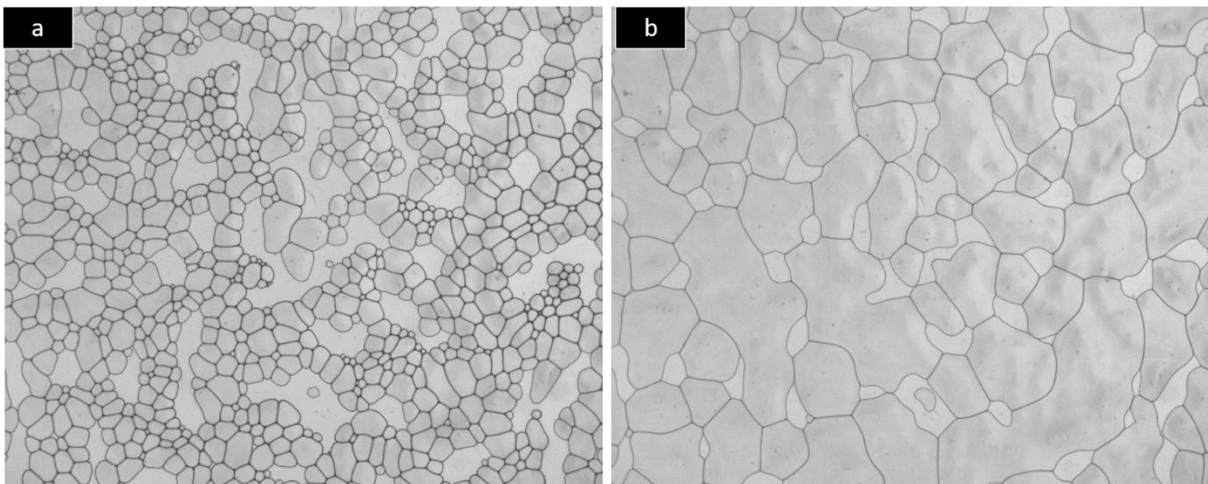


Figure 2. 7 a) The unprocessed image at the start of the coarsening experiment b)The unprocessed image after 24 hours of coarsening. The image size is 0.98 cm × 1.2 cm (Irregular model).

As mentioned before, to investigate the effect of fracture geometry on the coarsening phenomena, two fracture geometries have been used. The first model, with a regular pattern, and the second one, with

an irregular pattern. The first model is called the regular model, and the second one is the irregular model.

To observe the foam coarsening behavior of the entire fracture model, two various positions have been selected. One near the inlet shows the upstream behavior (Section 2 in figure 2.2), and the one near the outlet represents downstream behavior (section 5 in figure 2.2). All the experimental observations reported here have been carried out at these two positions. The average number of bubbles per pore and the average size of bubbles are two crucial parameters to monitor bubbles' coarsening rate over time. The experiments have been investigated with two different injected foam qualities. First, the "dry" case with the foam quality of 0.9, and the second, the "wet" model with the foam quality of 0.4.

In this chapter, to investigate the effect of geometry on the coarsening, only the dry foam with the foam quality of 0.9 has been considered. Due to gas diffusion, the bubble texture tends to coarsen with increasing time. Smaller bubbles disappear over time, losing their gas to surrounding bubbles until eventually, only one bubble is left per pore. Hence, the average number of bubbles per pore and the average size of bubbles are the two most essential parameters representing the coarsening rate in the fractured models.

As shown in figure 2.8, in the irregular model, at the beginning of the experiment, the bubble density in the downstream section was much greater than the upstream, 65 bubbles per pore in the downstream against 40 bubbles per pore in the upstream. However, as the coarsening time increased, the coarsening rate became slower and slower so that at the time of 10 hours, they reach a plateau. It means that a considerable number of tiny bubbles have been disappeared due to coarsening. The results show that the time of 10 hours is almost the time when the coarsening process for the irregular model became very slow. Increasing the average size of bubbles (figure 2.9) shows that the coarsening influenced the foam flow behavior. As the small bubbles disappear, the average size of neighbors becomes larger, so that coarsening rate becomes slower and slower. The effect of coarsening on foam behavior during the experiment is depicted in Figure 2.10.

It is worth mentioning that during foam coarsening in the irregular model, between 3 and 12 hours of coarsening, trains of bubbles occasionally flow from downstream to upstream. It was most likely caused by a small leak in the injection tube. However, in our study, these backflow events had no effect on the overall behavior of foam coarsening.

In contrast, the coarsening in the regular model showed a different behavior compared to the irregular model. Based on the bubble density in figure 2.8, the upstream and downstream behaviors were almost the same. However, compared to the irregular model, the coarsening was ended much sooner in the

regular model. As a result of the coarsening, the bubble density has been dropped until 5 hrs. According to figure 2.11, coarsening has been caused foam lamellae to move to low energy configurations in the pore throats and finally reaching one bubble per pore. Besides, the average size of bubbles confirms that when the coarsening rate is zero, bubbles' size becomes stable entire the fracture model, both in the upstream and downstream sections (figure 2.9). This time (5 hrs) can be considered the ending time of the regular model's coarsening. It is worth mentioning that fracture setup and optimum experiment time are two critical parameters in defining the coarsening's ending point. Both setup and experiment time should be long enough to reach equilibrium condition and monitor the coarsening phenomena.

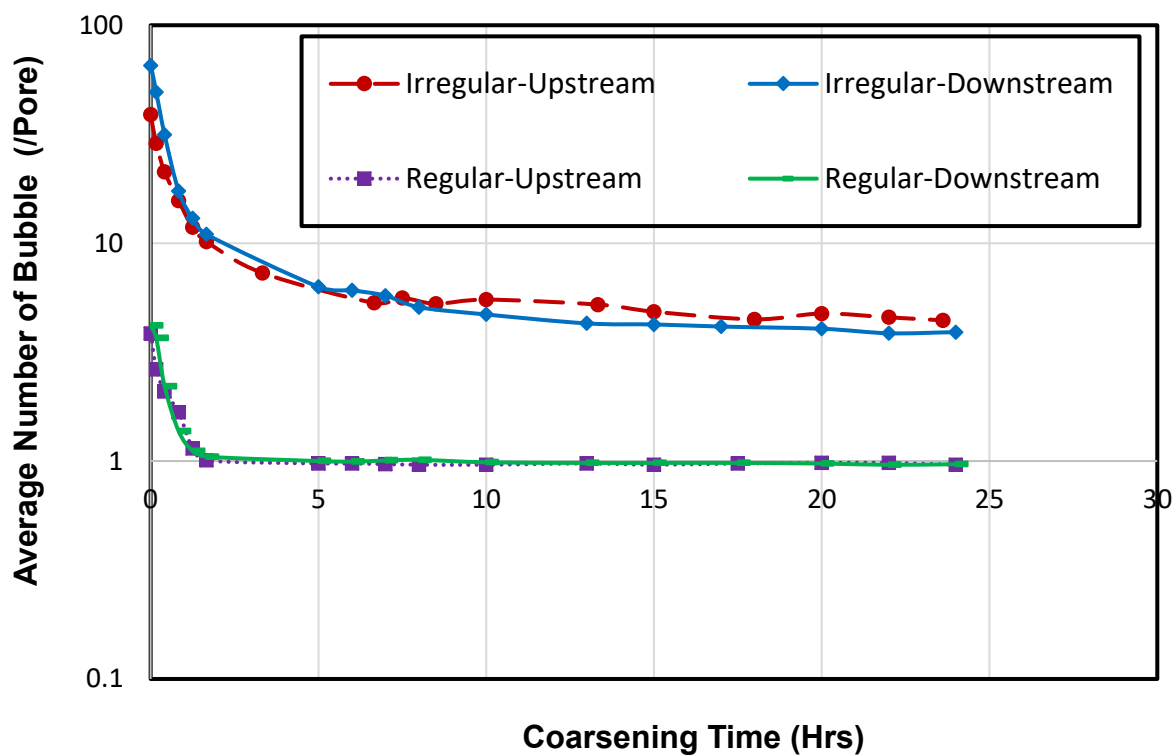


Figure 2. 8 The Average Number of bubbles in both regular and Irregular models in two various locations with the fg: 0.9

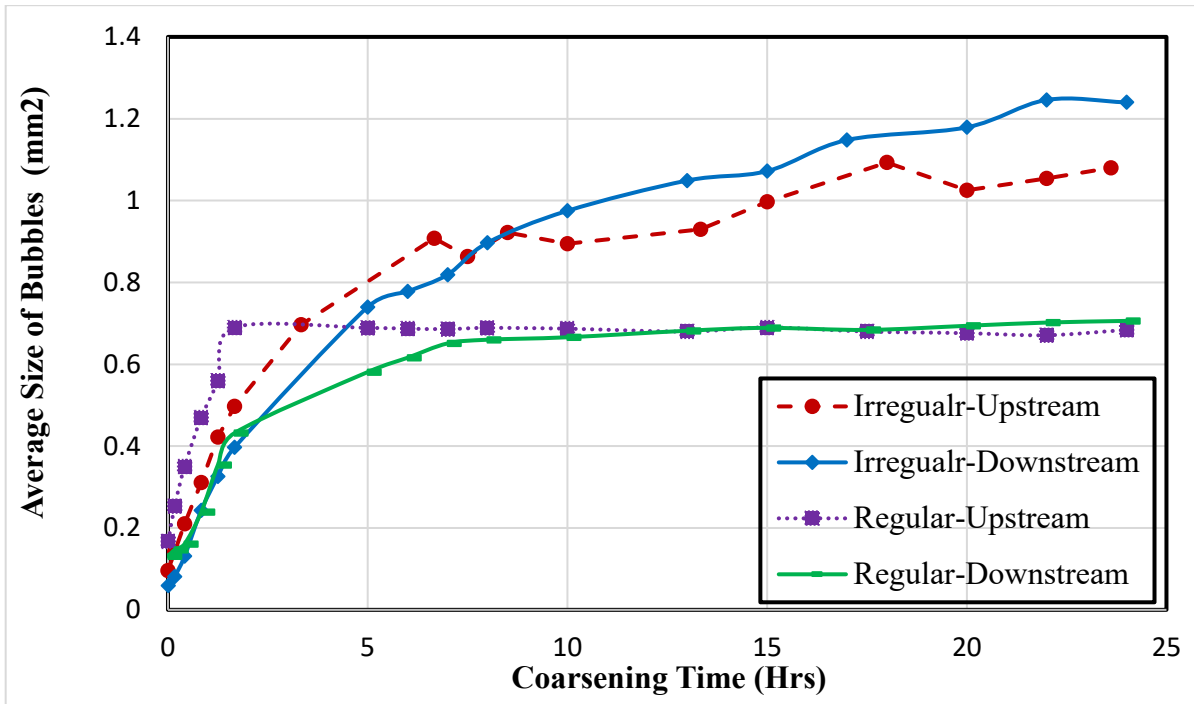


Figure 2. 9 The Average Size of bubbles in both regular and Irregular models in two various locations with the fg: 0.9

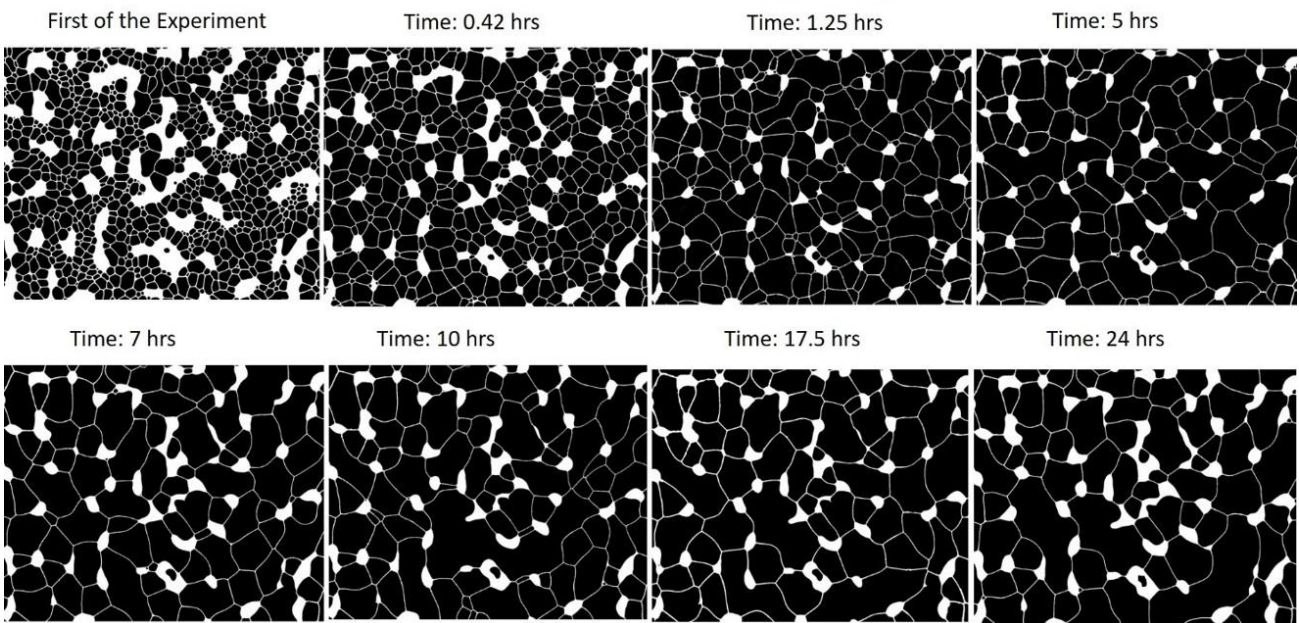


Figure 2. 10 The top view of the coarsening behavior through the Irregular model at upstream with the fg: 0.9. The image size is 0.98×1.2 cm. Black is gas and white is water (irregular model)

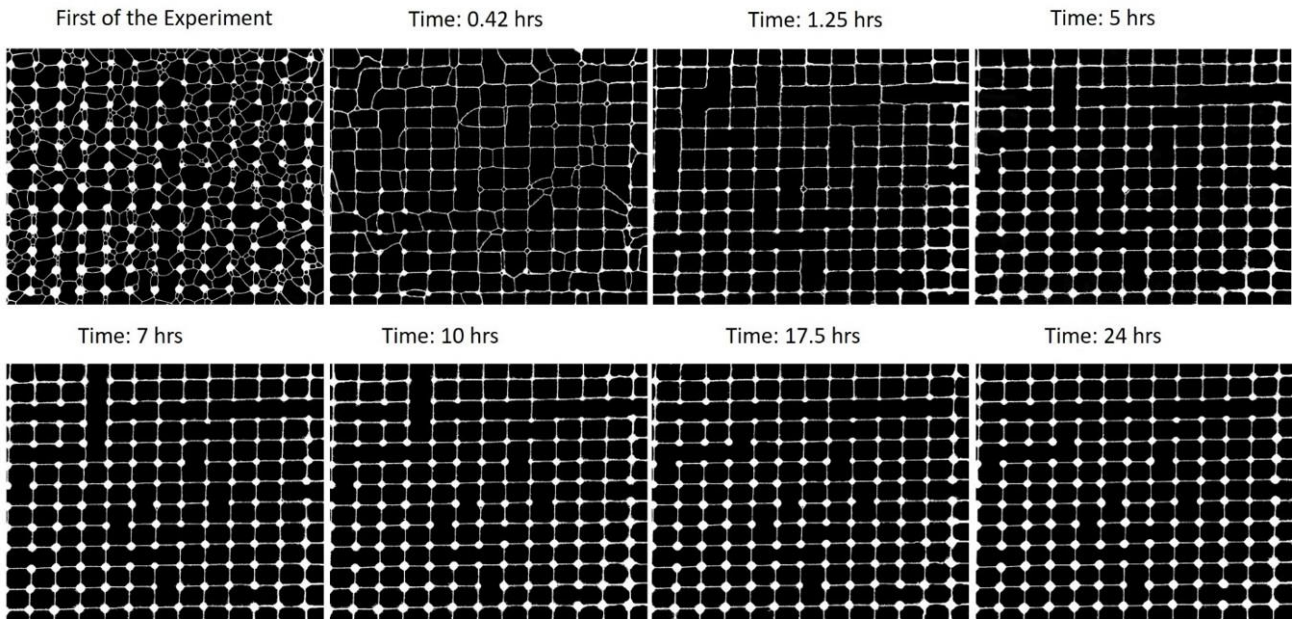


Figure 2. 11 The top view of the coarsening behavior through the regular model at upstream with the $fg: 0.9$. The image size is 0.98×1.2 cm. Black is gas and white is water (regular model)

2.4 Coarsening time scaling:

The fracture geometry is one of the critical parameters that can substantially impact the coarsening behavior and, in particular, coarsening time in micromodel structures. To confirm this effect, our model's results have been compared to the other two previous studies, done by [51] and [60].

In the Jones study, foam coarsening tests were carried out in a borosilicate-glass 2D micromodel. The micromodel was designed with an irregular hexagonal pattern that formed a porous medium, with a gaussian distribution of pore diameters (mean = 60 μm) and throat widths (mean = 13 μm). To investigate the behavior of coarsening through the fracture model, the ratio $\frac{N_0}{N_{t_c}}$ over coarsening time was measured, where N_0 is the initial number of bubbles and N_{t_c} is the number of bubbles at the time t_c . As can be seen in figure 2.12,

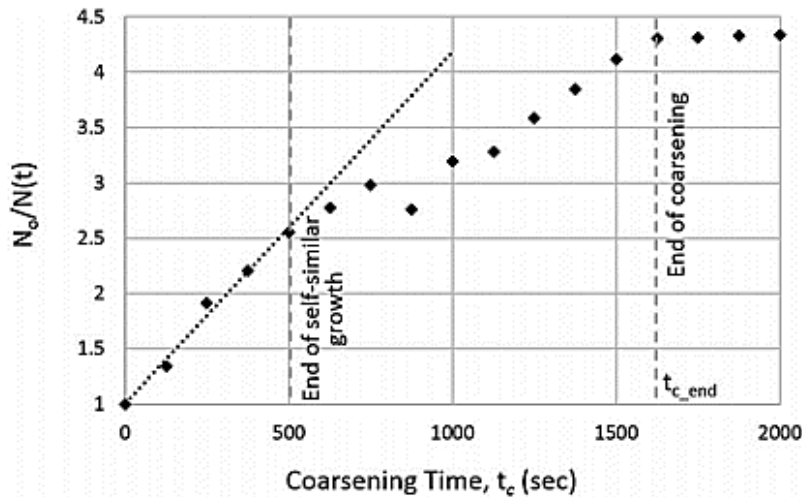


Figure 2. 12 The ratio of the initial number of bubbles, N_0 , to the number at time t_c , $N(t_c)$ plotted as a function of time, for a single coarsening test (representative of the general behavior seen in repeat tests). The experimental data deviate from the linear trend after approximately 500 seconds [51]

1. The coarsening was initially self-similar, which meant that the bubble structures' topology remained invariant with time. Linear growth of $N_0/N(t_c)$ was expected in this self-similar regime. Linear growth with time was also characteristic of the coarsening when there were no boundary effects.
2. A deviation from the linear growth was an indication of the situation when wall effects became significant. In this case, the boundary wall effect became noticeable after 500 seconds (end of self-similar growth indicated in Figure 2.12).
3. Finally, the coarsening stopped around 1600 seconds. At this time, most foam films were sitting in the pore throats, and it appeared that the bubbles were thermodynamically stable. The foam films had no curvature, which meant that the pressure drop between bubbles was nil, and consequently, gas diffusion was expected to be limited. Remarkably, the coarsening stopped after less than one hour, as this meant that the foam was expected to be stable for longer timescales.

In the second study on coarsening phenomena by [60], the experiments had been conducted on a microchannel with the dimension of $1500 \mu\text{m} \times 2500 \mu\text{m}$. In this paper, they built experiments on motionless microfoams, allowed for aging studies. A typical sample contained about 100 bubbles initially, some of which touched the container's boundary.

Figure 2.13 illustrates the number of internal bubbles as a function of time. A characteristic time could be defined for both populations of bubbles. Several effective diffusion coefficients led to

various slopes, probably corresponding to slightly different liquid fractions. From these curves, we extracted two characteristic times:

1. The time for which half of the bubbles disappeared, which they define as an order of magnitude of a characteristic time for practical issues in a standard situation (thickness of microfluidic system, size of storing chamber). This time was found to be around 2 or 3 minutes.
2. The time after which they could not extract pertinent information, due to a lack of statistics and due to boundary effects. Around 10 minutes, this time was characterized by the departure from the linear law in figure 2.13.

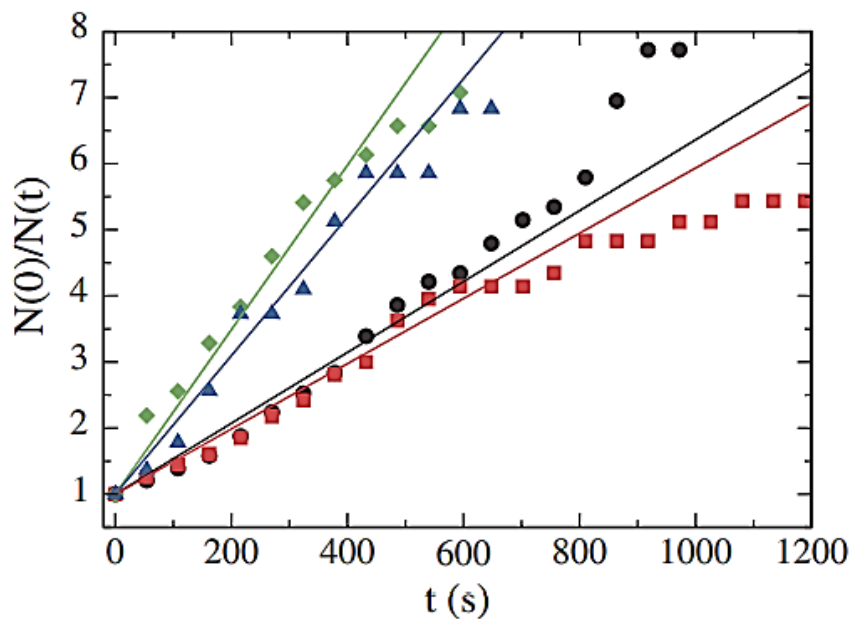


Figure 2. 13 Number of internal bubbles as a function of time. A characteristic time can be defined for both bubble populations [60] .

A normalized bubble density graph over coarsening time has been presented to compare our results with the mentioned studies.

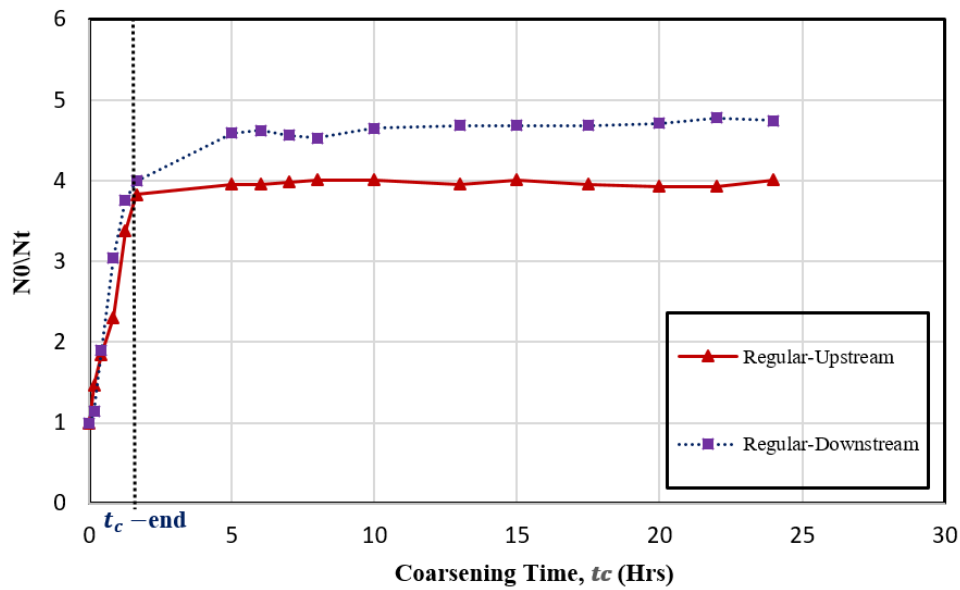


Figure 2. 14 The ratio of the initial number of bubbles to the number of bubbles at time t_c

Based on the regular model, after almost 5 hrs, the diffusion rate became constant, which meant that the coarsening was ended and the system reached the equilibrium condition. According to the results, it can be confirmed that the fracture's geometry can enormously change the coarsening rate. As shown in the mentioned studies, the coarsening can stop in the second, minute, or hour scale, based on the geometry structures.

2.5 The impact of the foam quality on coarsening:

The foam quality is the ratio of gas volume to foam volume (gas + liquid) over a given pressure and temperature. Nitrogen or CO₂ can create foam in liquid status, but nitrogen is typically preferred because CO₂ can be extremely harsh and eroding when water is existent.

To investigate the effect of foam quality on coarsening behavior, all the experiments have been conducted in the irregular model at two different foam qualities. First, a dry foam with the foam quality of 0.9, and then the wet foam with the foam quality of 0.4. In order to observe the behavior of the upstream and downstream, the tests have been carried out in two various locations, one near the inlet to show the upstream behavior and the one near the outlet to represent the downstream behavior of the static foam. As shown in figure 2.15, the bubble density of wet foam in the downstream was higher than the dry foam at the exact location. Besides, according to figure 2.16, two important observations could be mentioned. First, at the end of the coarsening experiment, the average size of bubbles for the wet foam in the downstream section was around 0.44 mm^2 , while for the dry foam in the same location was 1.24 mm^2 . Secondly, in the wet foam, bubbles have become stable in the middle of the experiment, which meant that the coarsening rate was much slower than the dry foam. The number of

bubbles decreased and bubble size increased as foam coarsened in both wet foam (fg 0.4) and dry foam (fg 0.9).

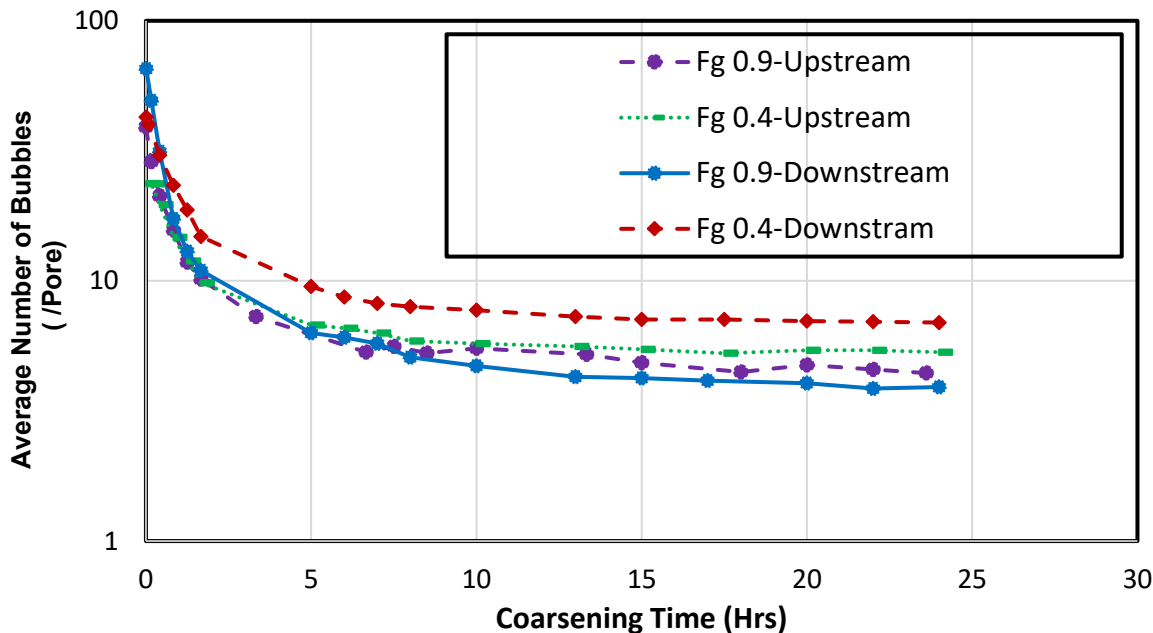


Figure 2. 15 The Average Number of bubbles per pore in two different locations of the irregular model with the two various ranges of foam quality

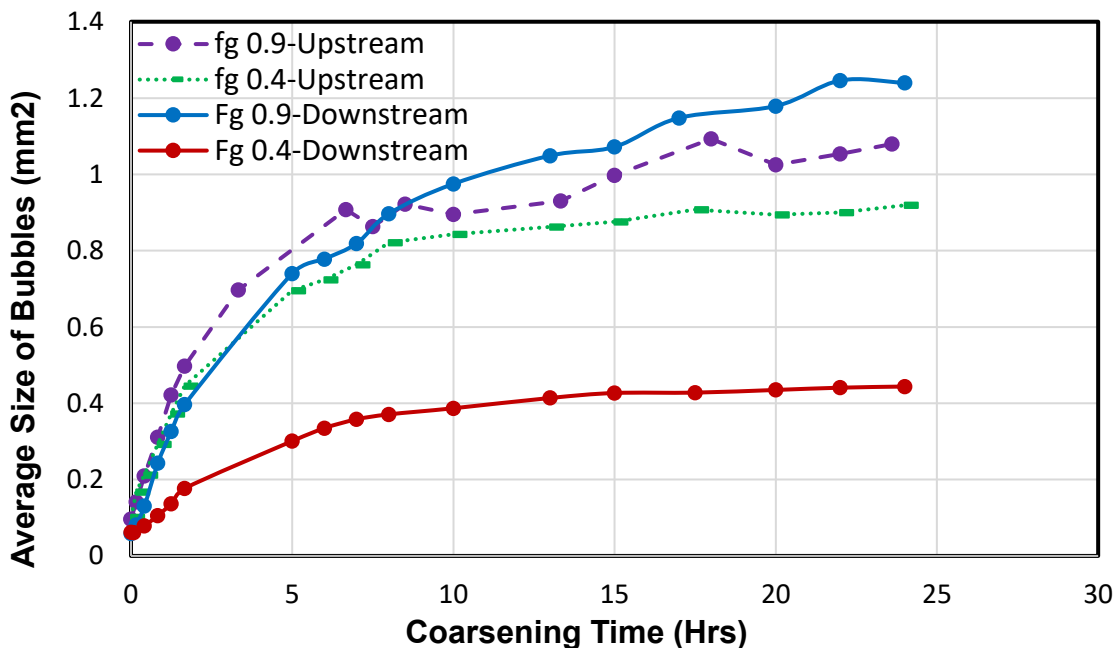


Figure 2. 16 The Average size of bubbles in two different locations of the irregular model with the two various ranges of foam quality

Figures 2-17 and 2-18 illustrate the behavior of the wet foam and dry foam, respectively. The gray patches represent gas bubbles, and white spots refer to the water phase. Hence, it can be concluded

that in the wet foam, due to the smaller size of the bubbles, diffusion happens sooner and the effect of coarsening on the static foam is much more vital than the dry foam. The effect on coarsening rate is because of the amount of water present. When there's more water, Capillary pressure is lower, Plateau borders are swollen, and there is less lamella area for diffusion.

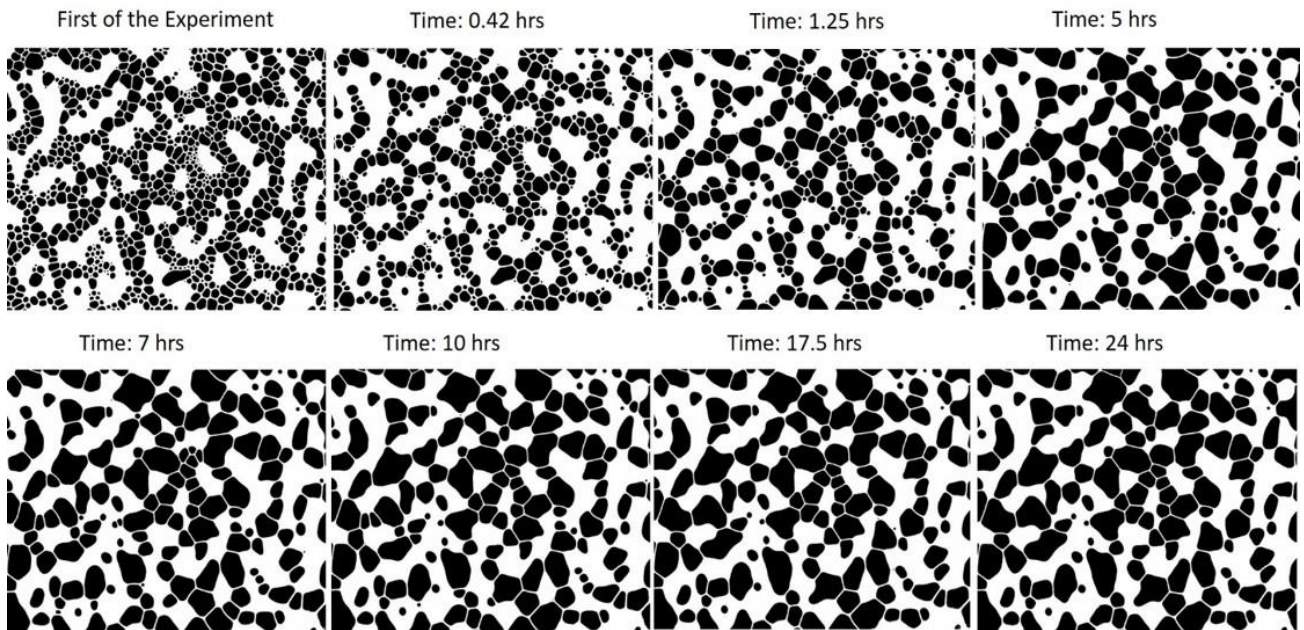


Figure 2. 17 The top view of the coarsening behavior through the Irregular model at downstream with the fg: 0.4 (wet foam)

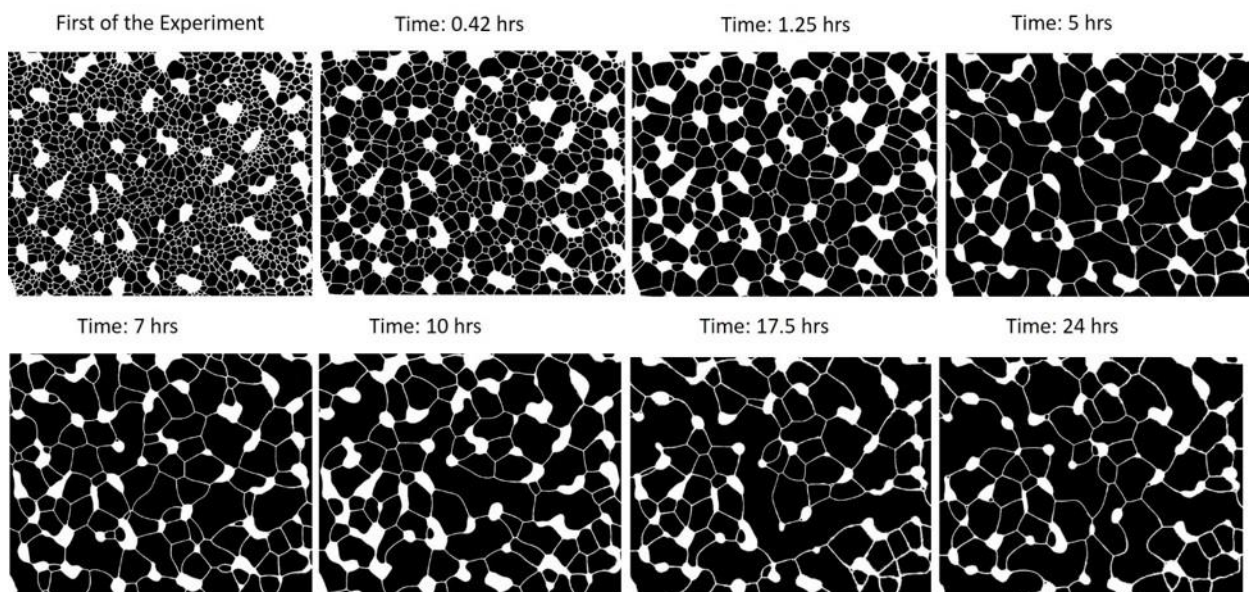


Figure 2. 18 The top view of the coarsening behavior through the Irregular model at downstream with the f_g : 0.9 (dry foam)

Chapter 3

Capillary Pressure Estimations through the Fully Characterized Physical -Model Fracture

3 Determination of Aperture Distribution

In order to determine the specific aperture from the height data, it is necessary to estimate the gap between the flat upper glass plate and the peaks in the roughed plate. We correlate the histogram of height on the roughened plate and water-occupied area fraction to estimate the aperture, where gas-water interfaces locate for a specific water-occupied area fraction. As shown in Figure 3.1, based on the x, y, and z coordinates measured by the chromatic profiler, the pixels' number over height values has been profiled in the regular model. In the next step, through the measuring cumulative pixel probability, represented as the cumulative gas area fraction, the specific aperture in each step concerning its particular gas area fraction has been calculated. In the final step, to calculate this aperture, the specific height of the cumulative pixel probability should be reduced from the maximum aperture value of the fracture. At the mountain peaks, which have the lowest value of the aperture, there is the liquid accumulation, and at the lowest points, having higher aperture values, gas can be accumulated. Figure 3.2 illustrates the histogram graph of the height values of the Irregular model.

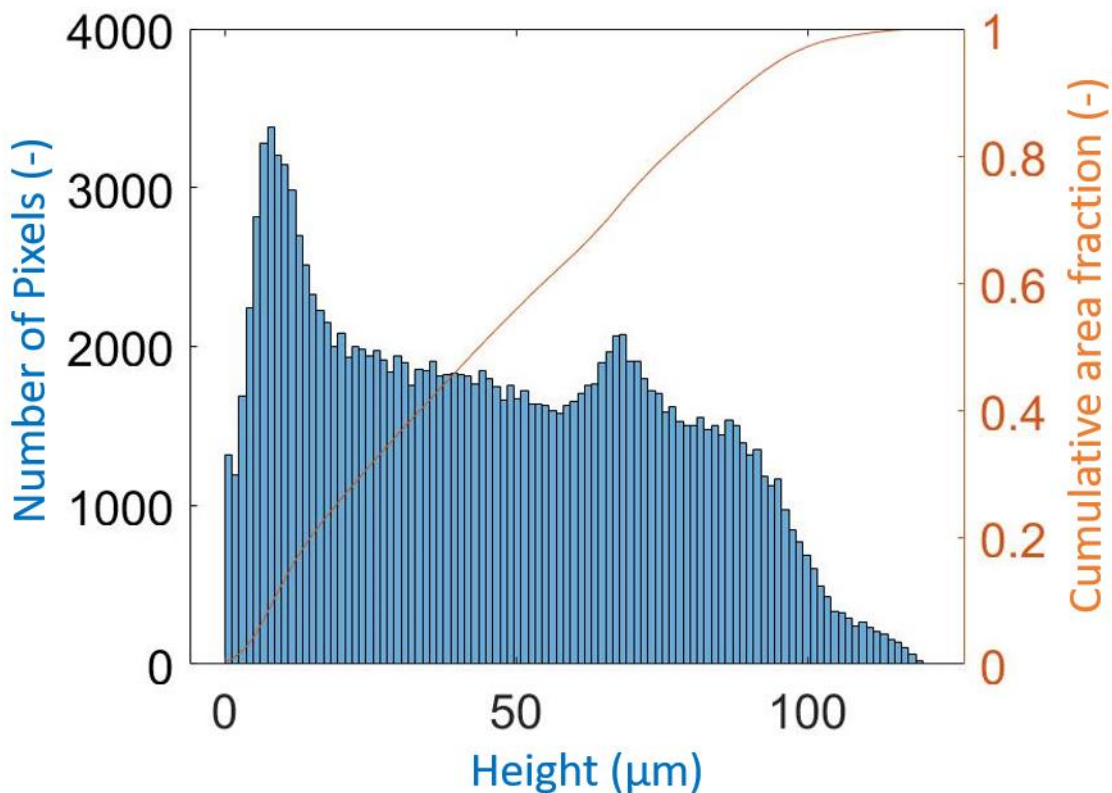


Figure 3. 1The Histogram graph of the regular model

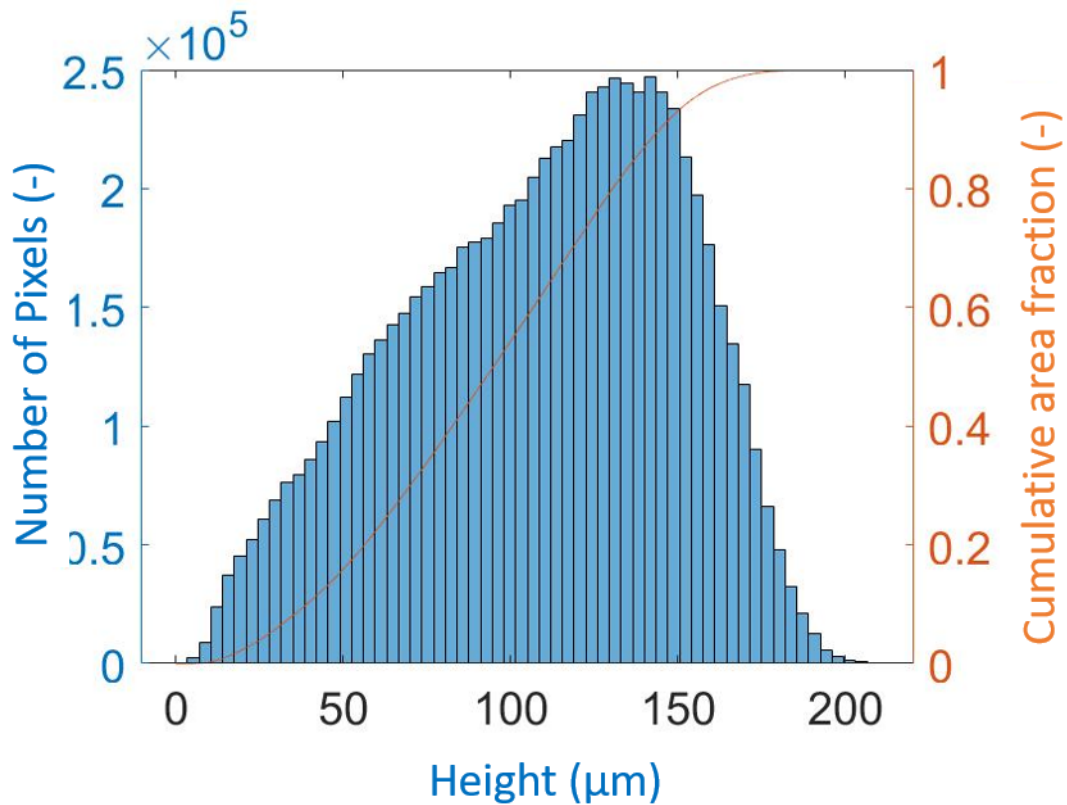


Figure 3. 2 The Histogram graph of the Irregular model

Tables 3.1 and 3.2 represent the specific aperture values for the regular model. As it can be seen, with increasing the gas area fraction, the aperture decreases. Since the gas area fraction in the dry foam is higher than the wet foam, the specific perture values in the dry foam are expected to be lower than the wet foam. To illustrate, in the regular model with the foam quality of 0.9, at the first of the coarsening experiment, where the gas area fraction was 76 %, the corresponding aperture was around 48 µm. In comparison, this value for the wet foam at the same time was approximately 67% due to its lower gas area fraction (59.6 %).

Table 3. 1 The Specific aperture values for the regular model- fg 0.9 at the downstream

Time (Hrs)	Gas Area Fraction	Corresponding Aperture (µm)
0.0083	0.7635	48.65
5	0.9269	29.194
10	0.9258	29.194
15	0.9333	27.977
20	0.933	27.977
24	0.9297	29.194

Table 3. 2 The Specific aperture values for the regular model- fg 0.4 at the downstream

Time (Hrs)	Gas Area Fraction	Corresponding Aperture (μm)
0.0083	0.596	66.903
5	0.823	42.574
10	0.9152	31.627
15	0.9065	32.843
20	0.8901	34.059
24	0.9	32.843

The Same calculations have been applied for the Irregular model. Tables 3.3 and 3.4 depict the corresponding aperture values for the irregular model. According to table 3.3, at the first of the coarsening experiment, the corresponding aperture at the gas area fraction of 67 % was 89 μm . After 24 hours of coarsening, since the foam became approximately 18 % drier, the aperture decreased to 59 μm .

Table 3. 3 The Specific aperture values for the irregular model- fg 0.9 at the downstream

Time (Hrs)	Gas Area Fraction	Corresponding Aperture (μm)
0.0083	0.6771	89.0759
5	0.8207	63.6256
10	0.8072	67.8673
15	0.7985	69.9882
20	0.8392	61.5048
24	0.8517	59.3839

Based on table 3.4, the wet foam became 18 % drier during the 24 hours of the coarsening experiment. The corresponding aperture at the first of the experiment was around 116 μm and, after 24 hours of coarsening, became 106 μm .

Table 3. 4 The Specific aperture values for the Irregular model- fg 0.4 at the downstream

Time (Hrs)	Gas Area Fraction	Corresponding Aperture (μm)
0.0083	0.4677	116.647
5	0.5038	112.4053
10	0.5261	110.2844
15	0.5333	108.1636
20	0.5371	108.1636
24	0.5403	106.0427

3.1 Capillary Pressure Estimation

We believe that in the fracture plane, the length scale in which the aperture differs is much greater than the aperture itself; hence, interfaces are almost cylindrical rather than spherical [61]. The curvature of the fracture is much greater than that of the fracture; therefore, the maximum capillary pressure during the passage through the throat can be written as follows [57]:

$$P_c = \frac{2\sigma \cos\theta}{d_t} \quad 3.1$$

where d_t is the minimum aperture, i.e., aperture at the throat. If we assume that the lamella is perpendicular to the contact wall, then the tangent line of the liquid film to the contact wall is 0 deg. Hence, the contact angle of 0 has been assumed in the capillary pressure estimations. Moreover, in this study, the interfacial tension between N2 and AOS surfactant solution was considered 32 dyne/cm.

In a porous medium, capillary pressure depends on the water saturation. Meanwhile, the gas fractional-flow function is a function of bubble size. At the limiting capillary pressure (P_c^*), foam breaks. It is assumed that the limiting capillary pressure differs with the form and concentration of the surfactant, electrolyte concentration, gas flow rate, and porous medium permeability [14]. However, it is not known the exact dependency on these variables.

Figure 3.3 shows the nonliniaer relation between the capillary pressure and the gas area fraction in the regular model. As can be noted, the capillary pressure estimates for both upstream and downstream sections at two different foam qualities have been calculated. As the foam quality increased, the specific aperture showed a higher value. Consequently, the capillary pressure increased. During the image analysis, it was argued that no lamella rapture was observed. Besides, the relatively small

capillary pressure values can confirm that the capillary pressures were lower than the limiting capillary pressure value in both regular and irregular models. Figure 3.3 depicts the estimated value of the capillary pressure for both sections at two different foam qualities in the regular model. In the wet foam in the downstream section, at the first of the experiment, the capillary pressure was 1.3 KPa, and almost after five hours, it reached a plateau at approximately 2.2 KPa. After a particular time, observing the constant capillary pressure can confirm that the lamellae positioned in the pore throat, where they had the minimum energy of the configuration, and consequently, the capillary forces became zero. According to the top view of the regular model showed in the previous chapter (figure 2.4), the purple patches show the cylindrical interphase with an aperture of approximately 50 μm . Considering the maximum height value (figure 1.3), which is 120 μm , the lamellae were most likely to position in the place with an aperture of around 70 μm .

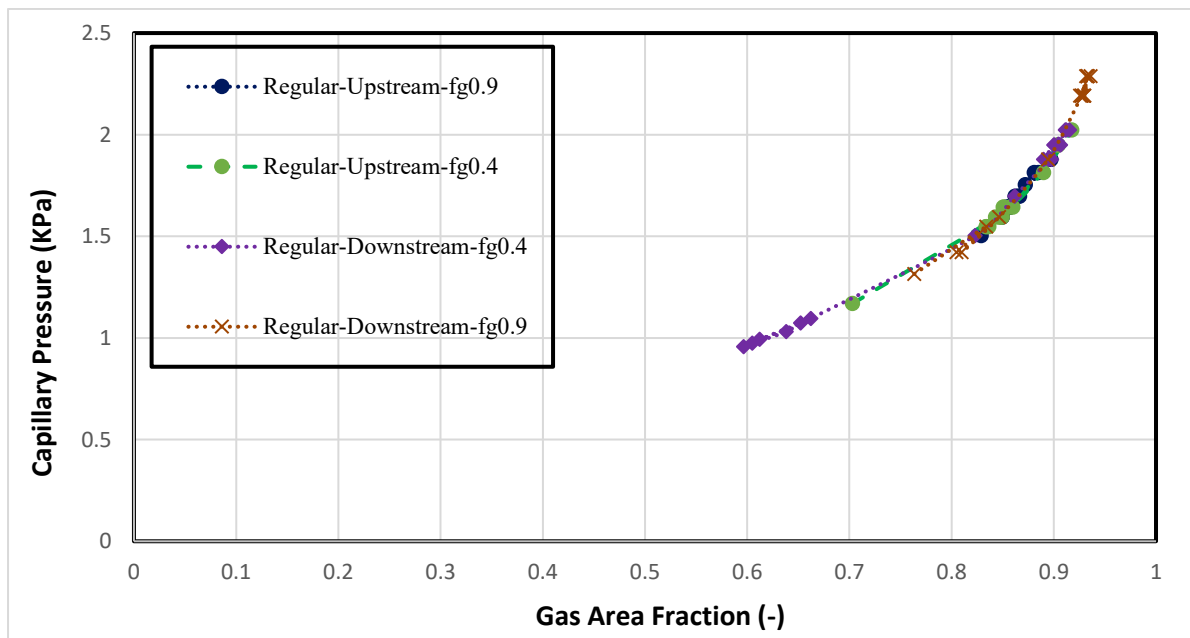


Figure 3. 3 The capillary pressure Estimation based on the gas area fraction at two various foam quality (Regular Model)

Figure 3.4 illustrates the capillary pressure over gas area fraction in the irregular model. As shown, since the capillary pressure has been estimated with the same formula (formula 1.3), their behaviors concerning the gas area fraction were the same for all sections. The capillary pressure ranges for the irregular model were much less compared to the regular model. To illustrate, at the end of the coarsening experiment, in the regular model, the capillary pressure in the dry foam in the upstream section was around 2.2 Kpa. In contrast, this value in the irregular model at the same location was approximately 1 KPa, which was almost two times smaller than the regular model. Figure 3.5 depicts the capillary pressure differences between two regular and irregular models.

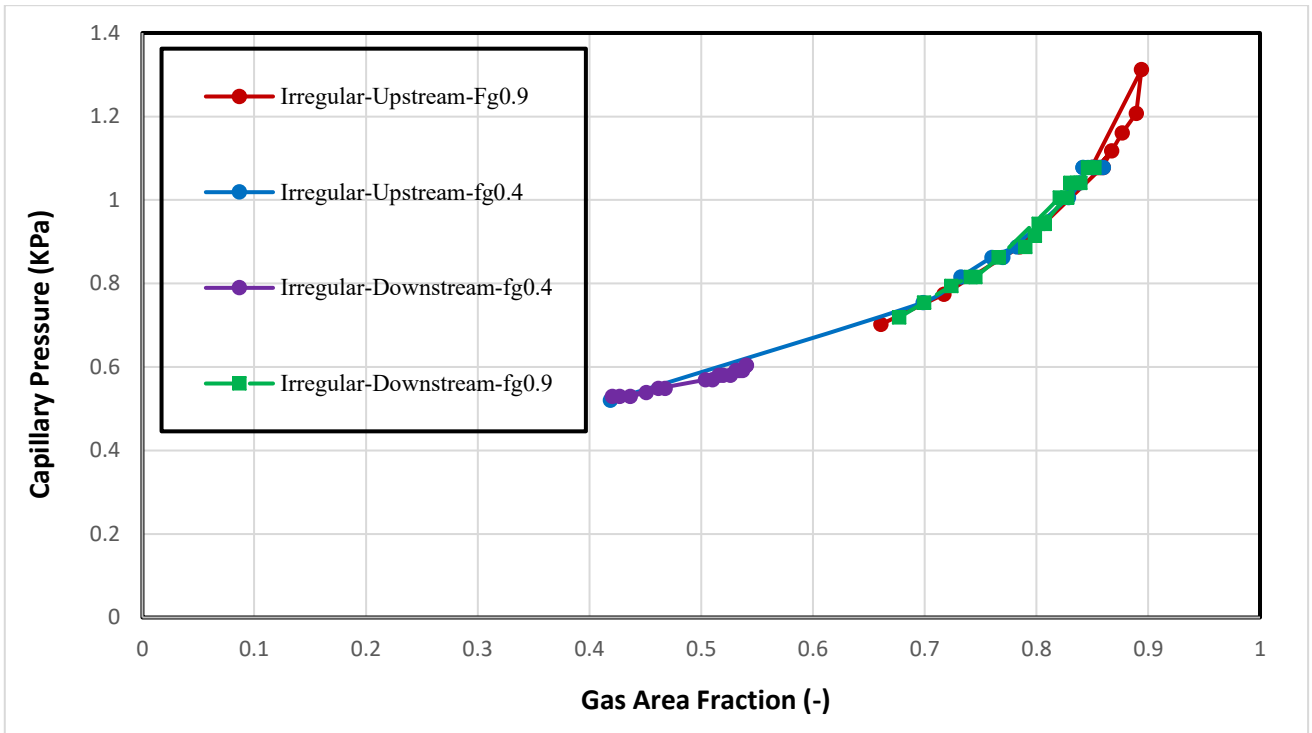


Figure 3. 4 The capillary pressure Estimation based on the gas area fraction at two various foam quality (Irregular Model)

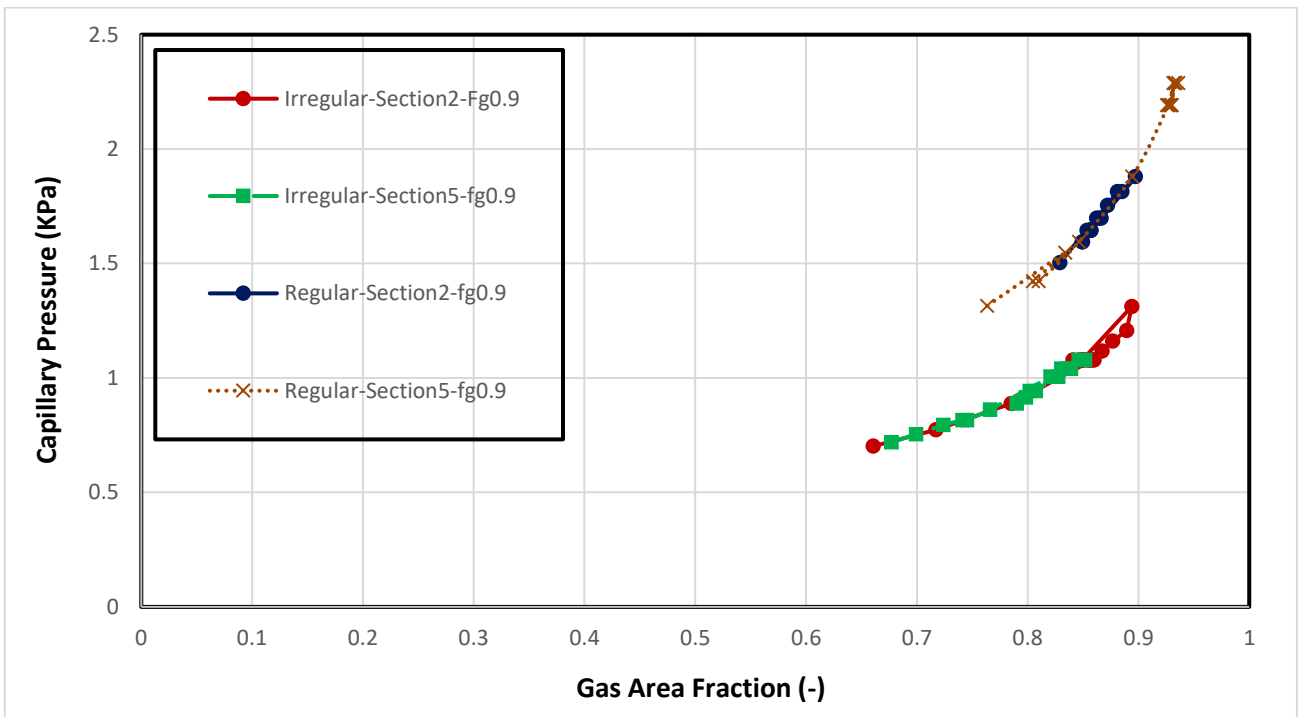


Figure 3. 5 Comparing the capillary pressure Estimation in both regular and irregular models

Chapter 4

Conclusions and Recommendations

4 Summary and conclusions:

In this study, the coarsening phenomenon has been studied in two fracture apparatuses made of glass plates. The ImageJ software has been used in order to analyze the raw images captured by the camera. All the experiments have been carried out in the two different sections at two various foam qualities. Based on the experiments, the following results have been concluded:

- The number of bubbles decreases and bubble size increases as foam coarsens in both regular and irregular model fractures.
- The average size of bubbles in the irregular model was much larger than the regular model.
- The coarsening ended much sooner in the regular model compared to the irregular model. the ending time of the coarsening was around 5 hrs, and it reached the equilibrium condition (one bubble per pore at the end of the coarsening experiment).
- In the irregular model, it concluded that after around 18 hours, the coarsening rate became very slow. Besides, since at the end of the coarsening experiment, there were four bubbles per pore, which can be supposed that the equilibrium condition has not been reached.
- The coarsening rate is strongly affected by fracture geometry, and it varies from minute to hour scale based on the various geometries.
- The effect of foam quality on the coarsening has been studied. The results depicted the number of bubbles decreases and bubble size increases as foam coarsens in both wet foam (fg 0.4) and dry foam (fg 0.9). Besides, there were two important observations from the average size of bubbles. First at the end of the experiment, the average size of bubbles for the wet foam at downstream is smaller than the dry foam. Second, in the wet foam, bubbles have become more stable in the middle of the experiment, meaning that the coarsening rate in wet foam is much slower than the dry foam.
- In order to measure the capillary pressure, both regular and irregular models have been profiled throughout the Matlab software. According to the results, capillary pressure values in both models were very small and not reaching the limiting capillary pressure.
- Although in our study some bubbles occasionally flow from downstream to upstream between 3 hours and 12 hours of coarsening, these backflow events had no effect on the overall behavior of foam coarsening.
- The capillary pressure ranges in the regular model were almost two times higher than the irregular models.

- Based on the regular model results, lamellae were most likely to position in the place with an aperture of around 70 μm .

Recommendations:

- In this study, the foam coarsening in a static foam has been studied in detail. However, the effect of coarsening in the dynamic foam has not still well defined.
- Since the fracture apparatuses were placed horizontally, the effect of gravity was neglected in our study. In the ongoing researche, the impact of gravity on the coarsening can be investigated.
- Other parameters can affect the coarsening phenomenon, such as the injection method. In future work, the impact of this parameter also can be taken into account.
- It is essential to find the practical application of such studies in the field.

References :

1. Lord, D., *Analysis of dynamic and static foam behavior*. Journal of Petroleum Technology, 1981. **33**(01): p. 39-45.
2. Ozbayoglu, M.E., et al. *A comparative study of hydraulic models for foam drilling*. in *SPE/CIM International Conference on Horizontal Well Technology*. 2000. Society of Petroleum Engineers.
3. Herzhaft, B., et al. *Aqueous foams for underbalanced drilling: The question of solids*. in *SPE Annual Technical Conference and Exhibition*. 2000. Society of Petroleum Engineers.
4. Bonilla, L.F. and S.N. Shah. *Experimental investigation on the rheology of foams*. in *SPE/CERI Gas Technology Symposium*. 2000. Society of Petroleum Engineers.
5. Okpobiri, G.A. and C.U. Ikoku, *Volumetric requirements for foam and mist drilling operations*. SPE Drilling Engineering, 1986. **1**(01): p. 71-88.
6. Beyer, A., R. Millhone, and R. Foote. *Flow behavior of foam as a well circulating fluid*. in *Fall meeting of the society of petroleum engineers of AIME*. 1972. Society of Petroleum Engineers.
7. Russell, B. *How surface hole drilling performance was improved 65%*. in *SPE/IADC Drilling Conference*. 1993. Society of Petroleum Engineers.
8. Farzaneh, S.A. and M. Sohrabi. *A review of the status of foam application in enhanced oil recovery*. in *EAGE Annual Conference & Exhibition incorporating SPE Europec*. 2013. Society of Petroleum Engineers.
9. Eren, T., *Foam characterization: Bubble size and texture effects*. Middle East Technical University, 2004.
10. Friedmann, F. and J. Jensen. *Some parameters influencing the formation and propagation of foams in porous media*. in *SPE California Regional Meeting*. 1986. Society of Petroleum Engineers.
11. Enick, R.M., et al. *Mobility and Conformance Control for CO₂ EOR via Thickeners, Foams, and Gels--A Literature Review of 40 Years of Research and Pilot Tests*. in *SPE improved oil recovery symposium*. 2012. Society of Petroleum Engineers.
12. Farajzadeh, R., et al., *Effect of permeability on implicit-texture foam model parameters and the limiting capillary pressure*. Energy & fuels, 2015. **29**(5): p. 3011-3018.
13. Vrij, A. and J.T.G. Overbeek, *Rupture of thin liquid films due to spontaneous fluctuations in thickness*. Journal of the American Chemical Society, 1968. **90**(12): p. 3074-3078.
14. Khatib, Z., G. Hirasaki, and A. Falls, *Effects of capillary pressure on coalescence and phase mobilities in foams flowing through porous media*. SPE reservoir engineering, 1988. **3**(03): p. 919-926.
15. Janssen, M.T., P.L. Zitha, and R.M. Pilus. *Oil Recovery by Alkaline-Surfactant-Foam ASF Flooding: Effect of Drive Foam Quality on Oil Bank Propagation*. in *SPE Improved Oil Recovery Conference*. 2018. Society of Petroleum Engineers.
16. Sheng, J.J., *Foams and their applications in enhancing oil recovery*, in *Enhanced Oil Recovery Field Case Studies*. 2013, Elsevier. p. 251-280.
17. Rossen, W.R., *Theory of mobilization pressure gradient of flowing foams in porous media: I. Incompressible foam*. Journal of Colloid and Interface Science, 1990. **136**(1): p. 1-16.
18. Rossen, W.R., *Foams in enhanced oil recovery*. Foams: theory, measurements and applications, 1996. **57**: p. 413-464.
19. Cantat, I., et al., *Foams: structure and dynamics*. 2013: OUP Oxford.
20. Feneuil, B., *Cement foam stability: link with cement paste rheological properties*. 2018, Université Paris-Est.
21. Farajzadeh, R., H. Bertin, and W.R. Rossen, *Editorial to the special issue: foam in porous media for petroleum and environmental engineering—experience sharing*. Transport in Porous Media, 2020. **131**(1): p. 1-3.

22. Kovscek, A., T. Patzek, and C. Radke. *Mechanistic prediction of foam displacement in multidimensions: A population balance approach*. in *SPE/DOE Improved Oil Recovery Symposium*. 1994. Society of Petroleum Engineers.
23. Hirasaki, G. and J. Lawson, *Mechanisms of foam flow in porous media: apparent viscosity in smooth capillaries*. Society of Petroleum Engineers Journal, 1985. **25**(02): p. 176-190.
24. Cohen, D., T. Patzek, and C. Radke, *Onset of mobilization and the fraction of trapped foam in porous media*. Transport in porous media, 1997. **28**(3): p. 253-284.
25. Géraud, B., et al., *The flow of a foam in a two - dimensional porous medium*. Water Resources Research, 2016. **52**(2): p. 773-790.
26. Rossen, W.R., *A critical review of Roof snap-off as a mechanism of steady-state foam generation in homogeneous porous media*. Colloids and Surfaces A: Physicochemical and Engineering Aspects, 2003. **225**(1-3): p. 1-24.
27. Chen, M., Y. Yortsos, and W. Rossen. *A pore-network study of the mechanisms of foam generation*. in *SPE Annual Technical Conference and Exhibition*. 2004. Society of Petroleum Engineers.
28. AlQuaimi, B. and W. Rossen, *Foam generation and rheology in a variety of model fractures*. Energy & Fuels, 2018. **33**(1): p. 68-80.
29. Kovscek, A., et al., *Foam flow through a transparent rough-walled rock fracture*. Journal of Petroleum Science and Engineering, 1995. **13**(2): p. 75-86.
30. Fernø, M.A., *Enhanced oil recovery in fractured reservoirs*. Introduction to Enhanced Oil Recovery (EOR) Processes and Bioremediation of Oil-Contaminated Sites, 2012. **89**(110): p. 89-110.
31. Gauteplass, J., et al., *Pore-level foam generation and flow for mobility control in fractured systems*. Colloids and Surfaces A: Physicochemical and Engineering Aspects, 2015. **468**: p. 184-192.
32. Johansen, S.A., *An experimental study of foam flow in fractured systems of increasing size*. 2016, The University of Bergen.
33. Ma, K., et al., *Visualization of improved sweep with foam in heterogeneous porous media using microfluidics*. Soft Matter, 2012. **8**(41): p. 10669-10675.
34. Osei-Bonsu, K., N. Shokri, and P. Grassia, *Foam stability in the presence and absence of hydrocarbons: From bubble-to bulk-scale*. Colloids and Surfaces A: Physicochemical and Engineering Aspects, 2015. **481**: p. 514-526.
35. Lemlich, R., *Prediction of changes in bubble size distribution due to interbubble gas diffusion in foam*. Industrial & Engineering Chemistry Fundamentals, 1978. **17**(2): p. 89-93.
36. Blijdenstein, T., P. De Groot, and S. Stoyanov, *On the link between foam coarsening and surface rheology: why hydrophobins are so different*. Soft Matter, 2010. **6**(8): p. 1799-1808.
37. Saint-Jalmes, A., *Physical chemistry in foam drainage and coarsening*. Soft Matter, 2006. **2**(10): p. 836-849.
38. Maestro, A., et al., *Foams stabilised by mixtures of nanoparticles and oppositely charged surfactants: relationship between bubble shrinkage and foam coarsening*. Soft matter, 2014. **10**(36): p. 6975-6983.
39. Exerowa, D. and P.M. Kruglyakov, *Foam and foam films: theory, experiment, application*. 1997: Elsevier.
40. Bhakta, A. and E. Ruckenstein, *Decay of standing foams: drainage, coalescence and collapse*. Advances in Colloid and Interface Science, 1997. **70**: p. 1-124.
41. Koczko, K., L. Lobo, and D. Wasan, *Effect of oil on foam stability: aqueous foams stabilized by emulsions*. Journal of colloid and interface science, 1992. **150**(2): p. 492-506.
42. Nikolov, A., et al. *The effect of oil on foam stability: mechanisms and implications for oil displacement by foam in porous media*. in *SPE annual technical conference and exhibition*. 1986. Society of Petroleum Engineers.
43. Osei-Bonsu, K., P. Grassia, and N. Shokri, *Effects of pore geometry on flowing foam dynamics in 3D-printed porous media*. Transport in Porous Media, 2018. **124**(3): p. 903-917.
44. Talebian, S.H., et al. *Foam assisted CO₂-EOR; concepts, challenges and applications*. in *SPE Enhanced Oil Recovery Conference*. 2013. Society of Petroleum Engineers.

45. Lobo, L., A. Nikolov, and D. Wasan, *Foam stability in the presence of oil: on the importance of the second virial coefficient*. JOURNAL OF DISPERSION SCIENCE AND TECHNOLOGY, 1989. **10**(2): p. 143-161.
46. Shojaei, M.J., *Pore-scale dynamics of foam flow in porous media*. 2020, University of Manchester.
47. Zolotukhin, A.B. and J.-R. Ursin, *Introduction to petroleum reservoir engineering*. 2000: Norwegian Academic Press (HóyskoleForlaget).
48. Skarestad, M. and A. Skauge, *Reservoarteknikk II, PTEK 213*. 2011, Fluid Properties and Recovery Methods.
49. Langlo, S.A.W., *Enhanced Oil Recovery by CO₂ and CO₂-foam Injection in Fractured Limestone Rocks*. 2013, The University of Bergen.
50. AlQuaimi, B.I. and W.R. Rossen, *Capillary desaturation curve for residual nonwetting phase in natural fractures*. SPE Journal, 2018. **23**(03): p. 788-802.
51. Jones, S., N. Getrouw, and S. Vincent-Bonnieu, *Foam flow in a model porous medium: I. The effect of foam coarsening*. Soft matter, 2018. **14**(18): p. 3490-3496.
52. Cohen, D., T. Patzek, and C. Radke, *Two-dimensional network simulation of diffusion-driven coarsening of foam inside a porous medium*. Journal of colloid and interface science, 1996. **179**(2): p. 357-373.
53. Weaire, D. and S. Hutzler, *The physics of foams*. Clarendon. 1999, Oxford.
54. Haugen, A., et al. *Experimental study of foam flow in fractured oil-wet limestone for enhanced oil recovery*. in *SPE Improved Oil Recovery Symposium*. 2010. Society of Petroleum Engineers.
55. Skoreyko, F.A., et al. *Understanding foam flow with a new foam EOR model developed from laboratory and field data of the naturally fractured cantarell field*. in *SPE improved oil recovery symposium*. 2012. Society of Petroleum Engineers.
56. Buchgraber, M., L.M. Castanier, and A.R. Kovscek. *Microvisual investigation of foam flow in ideal fractures: role of fracture aperture and surface roughness*. in *SPE Annual Technical Conference and Exhibition*. 2012. Society of Petroleum Engineers.
57. Alquaimi, B., *Investigation of foam generation, propagation and rheology in fractures*. 2017.
58. Chen, C.Y., R.N. Horne, and M. Fourar, *Experimental study of liquid - gas flow structure effects on relative permeabilities in a fracture*. Water resources research, 2004. **40**(8).
59. Yan, W., C.A. Miller, and G.J. Hirasaki, *Foam sweep in fractures for enhanced oil recovery*. Colloids and Surfaces A: Physicochemical and Engineering Aspects, 2006. **282**: p. 348-359.
60. Marchalot, J., et al., *2D foam coarsening in a microfluidic system*. EPL (Europhysics Letters), 2008. **83**(6): p. 64006.
61. Pruess, K. and Y. Tsang, *On two - phase relative permeability and capillary pressure of rough - walled rock fractures*. Water Resources Research, 1990. **26**(9): p. 1915-1926.

Tanzil, D. , "Foam Generation and Propagation in Heterogeneous Porous Media", Thesis for Ph.D., 2001

Appendix

According to tables A.1 and A.2, the capillary pressure estimation in both regular and irregular models, for whole sections have been presented.

Table A. 1 The Capillary pressure estimation for all sections in the regular model

Time (Hrs)	Pc (KPa) Upstream-fg 0.4	Pc (KPa) Downstream-fg 0.4	Pc (KPa) Upstream-fg 0.9	Pc (KPa) Downstream-fg 0.9
0.0083	1.169	0.956	1.503	1.315
0.4167	1.948	0.992	1.753	1.421
1.6667	1.948	1.096	1.879	1.879
5	1.644	1.503	1.697	2.192
8	1.594	2.023	1.644	2.192
10	1.644	2.023	1.644	2.192
13	1.644	1.879	1.644	2.287
15	1.594	1.948	1.644	2.287
20	1.594	1.879	1.644	2.287
22	1.547	1.948	1.594	2.287
24	1.547	1.948	1.594	2.192

Table A. 2 The Capillary pressure estimation for all sections in the irregular model

Time (Hrs)	Pc (KPa) Upstream-fg 0.4	Pc (KPa) Downstream-fg 0.4	Pc (KPa) Upstream -fg 0.9	Pc (KPa) Downstream-fg 0.9
0.0083	0.520	0.548	0.701	0.718
0.4167	0.815	0.529	0.887	0.794
1.6667	0.862	0.548	1.207	0.862
5	1.00	0.569	1.312	1.005
8	1.077	0.580	1.077	0.943
10	1.077	0.580	1.117	0.943
13	1.077	0.591	1.077	0.887
15	1.077	0.591	1.077	0.914
20	1.077	0.591	1.077	1.040
22	1.077	0.603	1.077	1.077
24	1.077	0.603	1.077	1.077